GENETIC ALGORITHM RECEIVER OPTIMIZATION FOR PASSIVE, BI-STATIC SYNTHETIC APERTURE RADAR

THESIS

Chad Nile Chamberlain, Major, USAF

AFIT-ENG-MS-17-S-007

DEPARTMENT OF THE AIR FORCE
AIR UNIVERSITY

AIR FORCE INSTITUTE OF TECHNOLOGY

Wright-Patterson Air Force Base, Ohio

AFIT-ENG-MS-17-S-007

GENETIC ALGORITHM OPTIMIZATION FOR PASSIVE, BI-STATIC SYNTHETIC APERTURE RADAR

THESIS

Presented to the Faculty

Department of Electrical and Computer Engineering

Graduate School of Engineering and Management

Air Force Institute of Technology

Air University

Air Education and Training Command

in Partial Fulfillment of the Requirements for the

Degree of Master of Science in Electrical Engineering

Chad Nile Chamberlain, B.S.E.E., M.S.O.R.

Major, USAF

14 September 2017

AFIT-ENG-MS-17-S-007

GENETIC ALGORITHM OPTIMIZATION FOR PASSIVE, BI-STATIC SYNTHETIC APERTURE RADAR

THESIS

Chad Nile Chamberlain, B.S.E.E., M.S.O.R.
Major, USAF

Committee Membership:

Dr. Julie A. Jackson
Chairman

Dr. Peter J. Collins
Member

Dr. Mark E. Oxley
Member

Abstract

Utilizing communication transmissions within an urban environment for passive radar has seen a huge surge in interest over the past decade. While the feasibility of using signals of opportunity for passive radar has been shown, very little research has been done for the optimization of passive transmitter/receiver pairings within urban environments. This research provides a receiver design based optimization of passive transmitter/receiver pairing using non-dominated sorting genetic algorithm II (NSGA-II) to solve a constrained multi-objective model. Comparing the results of an exhaustive search and the genetic algorithm (GA), the efficiency and effectiveness of using a GA for mixed variables over non-continuous, non-convex objectives associated with bi-static synthetic aperture radar (SAR) is demonstrated.

Acknowledgements

Many thanks to Dr. Julie Jackson for her devoted time and efforts on my behalf to direct me along the path of completion. I also would like to thank Dr. Peter Collins and Dr. Mark Oxley for their assistance, guidance and flexibility as Committee members. My thanks to Maj Andrew Compton for his help and direction with genetic algorithms, specifically with creating custom mutation and cross-over functions required to obtain the simulation results achieved by this research.

To my family, thank you for your patience, love and understanding along which became a difficult journey beyond the hardships expected.

Chad Nile Chamberlain

Table of Contents

List of Tables

List of Figures

Figure Page

GENETIC ALGORITHM OPTIMIZATION

FOR PASSIVE, BI-STATIC SYNTHETIC APERTURE RADAR

I. Introduction

Passive radar has seen an extremely large surge in interest as of late. The ability and effectiveness to use signals of opportunity from local digital broadcasts and cellular networks for passive radar have been extensively tested and shown [1–7]. With the ability of passively using local communication signals for radar, specifically synthetic aperture radar (SAR), the problem becomes not the availability of signals but the choice of which signal to use. Because the system user controls neither the transmitter signal nor transmitter parameters, limitations within the application and extent in use of the passive radar system arise. Recent studies [8–10] have shown that within any given passive radar scenario, certain transmitter/receiver pairings have advantages over others, based upon the application being exploited and the limitations placed upon the transmitters and/or receiver(s). The limitations could include location, flight path restrictions, operational frequency, bandwidth etc. Current studies approach the passive radar scenario from an optimal pairing choice or decision from an exhaustive search over definitive and finite parameters and constraints. This research approaches passive radar pairing optimization from a receiver design standpoint using a genetic algorithm (GA) to optimize a multi-objective model.

In radar applications, as with many other disciplines, often two or more desired objectives compete with each other. A simple example of two contradictory objectives is signal to noise ratio (SNR) and crossrange range resolution. As will be shown in

Chapter II, because both are functions of frequency, one cannot be optimized without degrading the other. This forced trade-off is most often the case when dealing with a multi-objective optimization.

Consider a simple multi-objective optimization (MOO) problem in the general form of

$$\boldsymbol{\gamma} \quad = \quad \begin{bmatrix} \boldsymbol{\gamma}_{opt_1} \\ \vdots \\ \boldsymbol{\gamma}_{opt_n} \end{bmatrix} \quad = \quad \underset{i=1,2,\cdots,n}{\text{argmin}} \quad F_i(\mathbf{x}) \quad \mathbf{s.t.} \quad G_j(\boldsymbol{x}) \underset{j=1,2,\cdots,m}{\overset{\leq}{=}} C_j \tag{1}$$

where $\mathbf{x}$ represents the vector of k design variables across the n objectives and the set of m constraints. A problem in the general optimization form of (1) could be relatively simple or complex. The n objective functions F_i could assume many different properties individually such as linear, non-linear, convex or non-convex and could be integer valued, discrete valued or continuous. The objectives may map into a complex field. The variables $\mathbf{x}$ upon which the objective functions are dependent could also be of mixed properties. If the objectives are simple, convex and continuous with variables that are not mixed, then the solution to the optimization could be achieved through a number of ways, such as an exhaustive search or gradient decent algorithm. As the complexity and interdependencies of objectives and variables increases, the solution space surface becomes more pitted and steeped. Simpler optimization methods such as gradient descent become unfeasible. The inability of simpler methods is due to computational complexity or an inability to solve reliably due to multiple local optimums across the objective space. Because radar has complex and often mixed variables and metrics, particularly bi-static SAR imagery formation, use of a genetic algorithm optimization is well suited.

The optimization of transmitter/receiver pairing has limited research. This research applies a multi-objective optimization of the form shown in (1) upon a simple passive bi-static synthetic aperture radar (PBSAR) scenario to identify trade-offs due to conflicting objectives. The optimization allows for various receiver configurations given established transmitter parameters. The objectives for the optimization within this research are derived from established bi-static metrics. A genetic program is used for the optimization of the multi-objective model. The receiver settings identified by the optimization are used to generate SAR images of a simple scene consisting of point scatterers. The images generated from the identified optimal settings are compared to illustrate the trade-offs between non-dominating points.

The remainder of this document is organized as such: Chapter II will discuss in more depth the current research relative to passive radar and transmitter/receiver pairing selection. Chapter II will also discuss the theory of optimization and bi-static radar. Chapter III will discuss the methodology used by this research to accomplish the optimization of the MOO model described herein. Chapter IV will show and discuss the results obtained by this research. Finally, Chapter V will discuss the conclusions drawn by the analysis of this research and discuss applications of future work.

II. Background

This chapter expands upon the problem of emitter selection and receiver optimization introduced in Chapter I, as well as discusses current research applicable to the optimization of a passive radar system. This chapter discusses various optimization methods generally used and the gaps within the published literature this research attempts to fill. It is assumed the reader has a basic understanding of radar operation, communication concepts, signal processing techniques and general optimization methods.

2.1 Passive Radar

Increasing demands for wireless public communication continually restrict the available frequency space. The past several years have seen a marked rise in the exploration of using communication signals for radar implementations. The feasibility of using an orthogonal frequency multiplex division (OFDM) communication signal within a radar application is well established [11–22] with particular interest in digital video broadcasting (DVB), digital audio broadcasting (DAB), world wide interoperability for microwave access (WiMAX), and long term evolution (LTE) signals [4, 8, 23–35]. With the defined ability to use communication signals in PBSAR and passive multi-static synthetic aperture radar (PMSAR), the problem of how to optimally configure receiver settings to optimize radar applications arises.

The decision problem of which transmitter(s) a receiver should pair with to optimize available data is depicted in Figure 1. A single receiver located within an urban environment that contains many transmitters has multiple pairing choices. While the optimal receiver configuration across several metrics could be simply computed for

a few transmitters through an exhaustive analysis, adding additional receivers and several transmitters quickly prevents a timely solution through an exhaustive search.

One reason for the the heightened interest in using communication signals for radar application is the increasingly crowded spectral space. As communication methods increase with the advances in communication signals and methodologies, the available spectrum for radar use becomes increasingly tightened. The Spectrum Sharing Innovation Test-Bed by the National Telecommunications and Information Administration (NTIA), Federal Communications Commission (FCC) and Federal agencies is one example of the efforts to improve spectral management of national airwaves [36]. With such a potentially dense spectral coverage of communication signals in urban environments, determining which signals of opportunities will yield the greatest results becomes a concern.

Optimization across the field of radar is continuously a topic of interest, whether it be the optimization of detection [37], the optimization of a waveform [1,37–39], or the optimization waveform selection [40]. Even an optimal receiver path to identify and track moving targets for an active multi-static system consisting of a single transmitter and multiple receiver has been examined [41]. A recent study was conducted examining the optimization of a SAR image by exhaustively searching the available pairings for a marine receiver with terrestrial communication transmitters [42]. Most recently a fast wide-area passive synthetic aperture radar (PSAR)/inverse synthetic aperture radar (I-SAR) performance prediction was looked at [43], where the performance of a system was tied to a single indicative metric of point spread function (PSF). There is, however, very limited research into the optimization of receiver design for a PBSAR system.

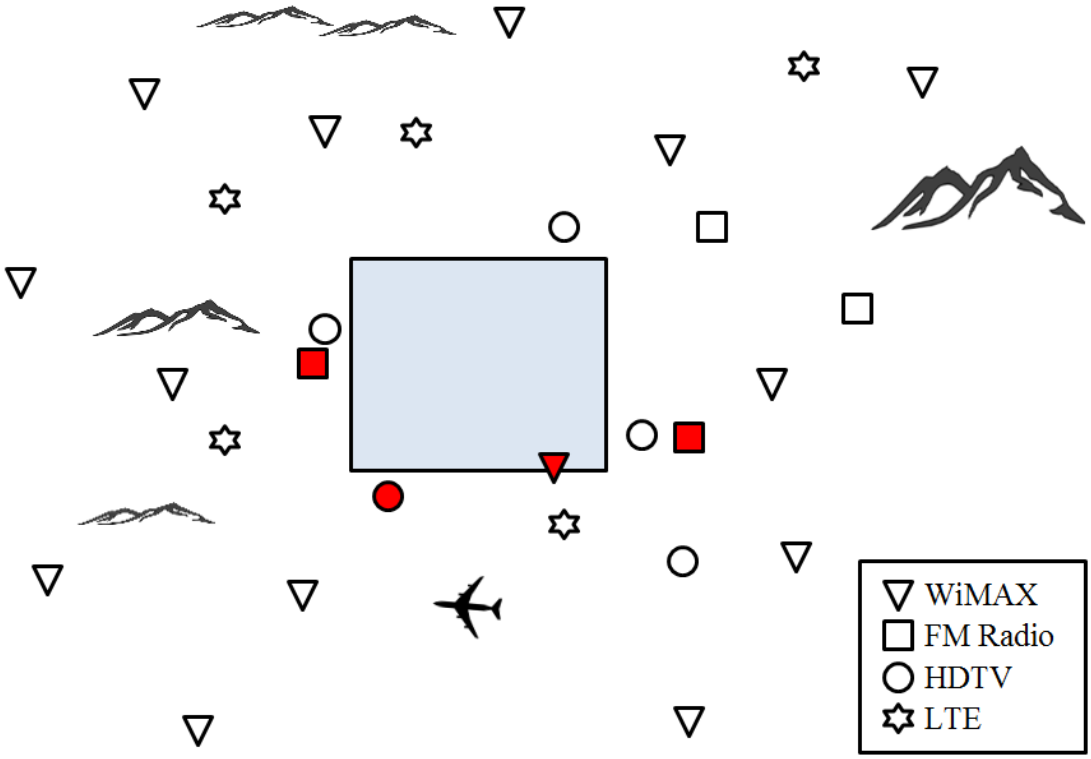

Figure 1. A multi-channel receiver needing to image the scene defined by the square has many transmitters to choose from. Each transmitter has unique parameters which the receiver accepts once it is matched to that transmitter's frequency.

An initial attempt upon emitter selection criteria optimization for a PMSAR was accomplished by Stevens [9]. A receiver with a fixed flight path and flight duration within an environment of 24 transmitters of various signal types was optimized for up to 4 possible receiver channels. The optimization was based upon a weighted utility function defined by five metrics: multi-static signal to noise ratio (MSNR), effective multi-static resolution area (EMRA), ambiguity function integrated side-lobe level (AF-ISL), point target contrast ratio (PTCR) and distributed target contrast ratio (DTCR). The derivation of the metric definitions were a major part of the work and the calculations were extensive for many of the metrics. The metrics were shown to contribute to the defined quality of a SAR image. The feasibility of a pairing was preselected against two requirements: (i) adequate SNR and (ii) frequency overlap between receiver and transmitter operating frequencies. With the defined constraints of up to 4 receiver channels, SNR above -30 dB and frequency overlap, there were 2680 possible combinations. The selection criteria was evaluated through an exhaustive search and produced a ranked ordering for all feasible transmitter(s)/receiver combinations. While Stevens' work evaluated possible pairings of platforms with fixed parameters, this research examines the optimization of pairings by allowing receiver parameters to vary.

This research furthers the aforementioned emitter selection work into a general constrained multi-objective optimization of receiver design. The focus of the optimization begins with the optimization of a single receiver across two variables with five transmitters of opportunity, building up to multiple receivers with flight paths that can be varied in the x-y plane. The optimization optimizes bi-static SAR image quality as determined by defined metrics within the constrained multi-objective

optimization.

2.2 Optimization Methods

Generally, optimization has been an area of interest for decades and as such there are many differing types of optimization methods. Many classical methods include exhaustive search, analytical, simplex, line minimization, weighted sum, Benson's Method and value function, to name only a few [44, 45]. Regardless of the method all optimizations have a few things in common. All methods assume there is some cost associated with the problem. The currency of the cost could be time, asset usage, or a metric of performance. All optimization methods assume there is a known mathematical representation of the cost function and is often called an objective or objective function. The objective is often parcel to certain constraints that limit the domain of the inputs or limit the range of the objective. All optimization methods are searching the objective or cost space to find the optimal value [44].

Optimization in its simplest form can be described as the pair f and X. Let f be the cost or objective function that maps the set of possible solutions X into the set of real numbers: $f : X \rightarrow \Re$. To find the global minimum of X means there exists some $s^* \in X$ such that $f(s^*) \leq f(s)$ for all $s \in X$. The optimal cost is then $f(s^*)$ with s^* being the optimal solution. Often the default of optimization is to minimize, but the mathematical generality of doing so is not lost as you can simply say $f(s^*)$ $\geq f(s)$ for all $s \in X$ [45]. Figure 2 illustrates the mapping relationship between X and f.

One of the simplest methods for optimization is analytical optimization, also known as gradient descent. With gradient descent, as with many of the simpler

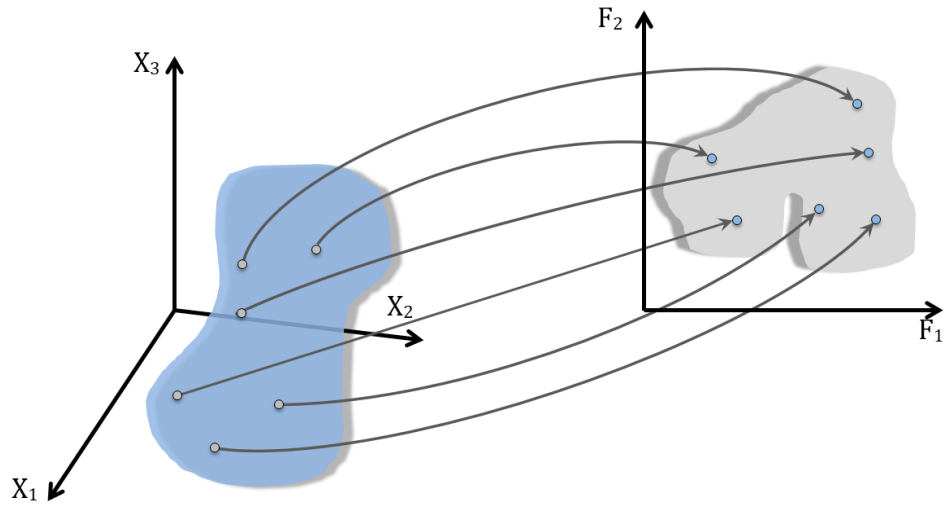

Figure 2. Graphical representation of the mapping from the decision space (X_1, X_2, X_3) to the objective space (F_1, F_2).

optimization methods, a smooth function $f(s)$ or differentiable function is assumed for all of $s \in X$. Finding the roots of the first function gradient $\Delta f(X)$, identifies the extrema and a simple search across all extrema can yield the global optimum within the space defined by $f(X)$ subject to all applicable constraints. However, not all gradient decent models complete a search across all possible gradient roots and often lead to a local optimization.

Most often optimization problems are "hard" problems consisting of multi-objective, non-continuous, non-linear, non-convex functions and/or design spaces [45]. Traditional methods cannot be applied to obtain solutions that are reliable and exact. Modern strategies examine the search space yielded by the domain of X to discover desirable solutions to the objective(s). Evolutionary algorithms, also known as genetic algorithms, have proven very adept and successful at exploiting the search space of complicated and difficult problems [46].

2.3 Genetic Programming

Evolutionary program, or genetic programming research lies within the discipline of computer science, but has implication and use across all research disciplines. Genetic programming research thus lies way beyond the scope of this research; as such we will present a basic tutorial of its beginnings and terminology necessary to understand the implementation and use of the GA used in this work, Matlab's® *gamultiobj*.

Genetic programming (GP) has seen exponential growth in interest since 1989 when the first literature on the subject was published. Only one article on genetic programming (GP) was published in 1989, compared to an estimated 13,000+ in 2016 across all disciplines [47]. GP has more in common with the selective breeding method proposed by Mendel than it does with classical optimization methods. The name genetic programming and much of the terminology arises from the commonness with selective breeding and Darwinism [46].

Figure 3 shows the basic progression of a genetic algorithm program. The program generates an initial group of solutions, a subset of X, which is called the population. This initial population draw can be done at random, from a priori knowledge or from the results of an earlier run. The a priori knowledge typically comes from the constraints placed upon the optimization problem or from user preference/knowledge. The members of the population are evaluated against the objectives. Some of the population is selected based upon the resulting objective values for the evaluation. At this point one generation within the algorithm has been completed. If the selected members of the population constitute a sufficient solution based upon defined algorithm termination conditions, the program stops. If the selection does not result in a sufficient solution, another population is generated and the process repeats

until termination conditions are achieved. The "new" population begins the second generation and are the children of the first or parent generation. The population for the"new" generation is created through the use of mutation and crossover criteria against members of the parent population.

Crossover is defined as the making of a new single population member by using some of the attributes of two members from the previous population exactly as two parents have a child. The child will share some of the genetic attributes of both parents. From a code standpoint, the crossover point directs where the algorithm splits the coded gene of each parent. For floating point numbers the crossover works as such. If the crossover point is "3", the offspring is set at "2", and the parents are respectively:

$$\mathbf{x}_{\text{dad}} = \left[\begin{array}{c} 1 \\ 2 \\ \hline 5 \\ 1 \\ 8 \\ 3 \end{array}\right] \qquad \mathbf{x}_{\text{mom}} = \left[\begin{array}{c} 0 \\ 7 \\ \hline 4 \\ 6 \\ 0 \\ 1 \end{array}\right]$$

the resulting children are

$$\mathbf{x}_{\text{kid}_1} = \left[\begin{array}{c} 1 \\ 2 \\ \hline 5 \\ 6 \\ 0 \\ 1 \end{array}\right] \qquad \mathbf{x}_{\text{kid}_2} = \left[\begin{array}{c} 0 \\ 7 \\ \hline 4 \\ 1 \\ 8 \\ 3 \end{array}\right]$$

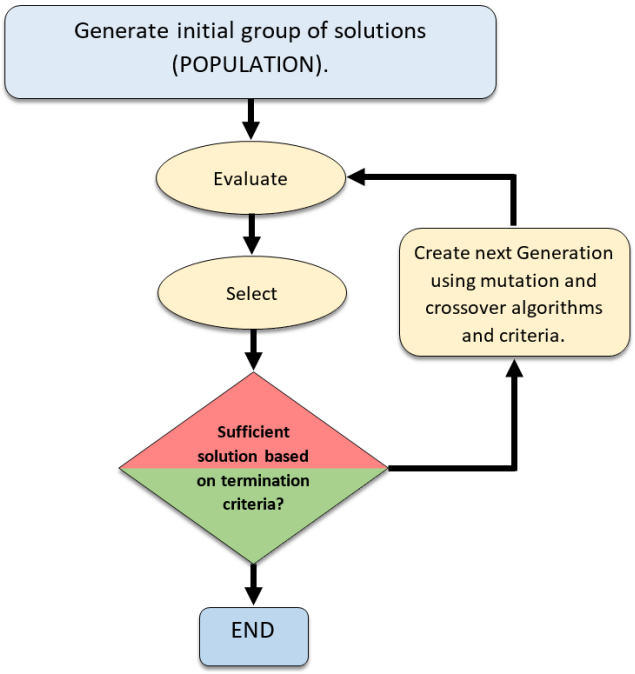

Figure 3. Flow chart for a basic genetic algorithm.

where the horizontal bar indicates the crossover point. Typically, crossover algorithms utilize two "selected" population members in an attempt to select for the desired attributes the parents exhibited, much as Mendel's selective breeding. However, crossover can occur between "non-selected" parents or one "selected" and one "non-selected" depending on the algorithm and crossover function settings.

Mutation is just as it sounds; some of the attributes from one or more members of the previous population are altered slightly to produce new attributes for a single population member. Mutation typically occurs for those members of the population not selected in an attempt to retain a diverse population. Maintaining a diverse population is critical for the GA's ability to avoid basins of attraction and maintain searching the entirety of the objective space. Both crossover and mutation algorithms can be customized in most GP programs.

The selection criteria for the population, as discussed above, is accomplished based upon the dominance or rank of the population members. Dominance deals with the n objective functions of a MOO such as that presented in (1). The $\lhd$ operator is used to denote that $a \lhd b$ means a is better than b for generality to cover both minimization and maximization objectives. Using this notation, solution dominance is defined as: [45]

Solution x_1 dominates solution x_2 if both conditions 1 and 2 are true:

$$\begin{aligned} &1. \quad f_i(x_1) \not\rhd f_i(x_2) \quad \forall \quad i = 1, 2, \cdots, n \\ &2. \quad f_i(x_1) \lhd f_i(x_2) \text{ for at least one } i \in 1, 2, \cdots, n. \end{aligned} \tag{2}$$

This means that solution x_1 is no worse than solution x_2 in all objectives and solution x_1 is strictly better than solution x_2 for at least one objective.

Based on the definition of dominance, there are exactly three outcomes of a dominance check between any two solutions. First, solution 1 dominates solution 2, second, solution 1 gets dominated by solution 2 and third, neither 1 nor 2 dominates the other solution. The third condition creates a situation often found when optimizing across two conflicting objectives, like that of SNR and cross range resolution, pointed out in Chapter I. Figure 4 shows the plot of 11 various points in the objective space. Since function F_1 is optimal at a maximum value, a point further right of any other point dominates with regard to objective F_1. F_2 is optimal at a minimum value, thus any point below of any other point dominates with regard to objective F_2. Comparing points 1 and 2, in Figure 4 we can see that point 2 dominates point 1 in both F_1 and F_2, since point 2 is better than point 1 in both objectives. Point 2 is larger (further to the right) for objective F_1 and smaller (lower) across the vertical axis, F_2. Comparing

points 3 and 5, however, we see that neither solution dominates the other. Point 3 is lower than point 5 and dominant in F_2, but point 5 is further right of point 3 and dominant in F_1. Being better in one objective but being worse in at least one other objectives brings about the concept of non-dominance.

Given a finite solution set X, all pair-wise comparisons can be made across the objective space. If we compose a set of solutions P which contains all the non-dominated solutions across the entire set of X, P constitutes the Pareto set or Pareto-optimal set [45]. Since it is assumed that all objectives within the MOO are important, it is not possible to say which solutions contained in P are better then the others in P. One solution will improve across one or more objectives, but deteriorate in one or more of the remaining objectives. The Pareto set is used to describe the portion of the search space where non-dominance occurs. The connection of these solutions within the search space constitutes the Pareto front. Figure 5 illustrates the Pareto front for the four different combinations of objective types across the same search space, namely min-min, min-max, max-min and max-max. The designation of the Pareto front gives the user options for a solution, and is one of the major advantages of GPs.

When dealing with a complicated, multi-objective problem, GPs have been proven to be effective. Haupt [44] shows the efficiency and effectiveness of a GP through an example of locating the highest peak in a specified section of the Rocky mountains, namely the Rocky Mountain National Park in Colorado. Using a quantized contour map 128 $\times$ 128 in size, the GP finds the optimal solution, Long's Peak. An exhaustive search would require 128 $\times$ 128 = 16,384 objective evaluations, while the GP took only 29 objective function evaluations, 0.18% of an exhaustive search. Haupt

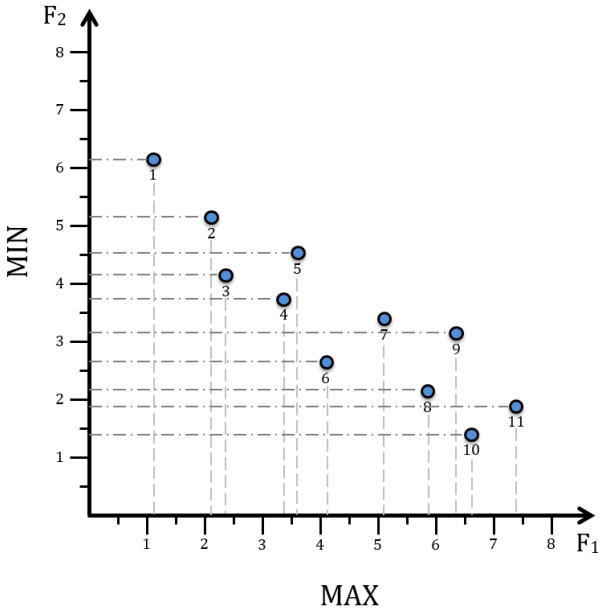

Figure 4. Solution population for a max-min optimization. Figure modeled after [45].

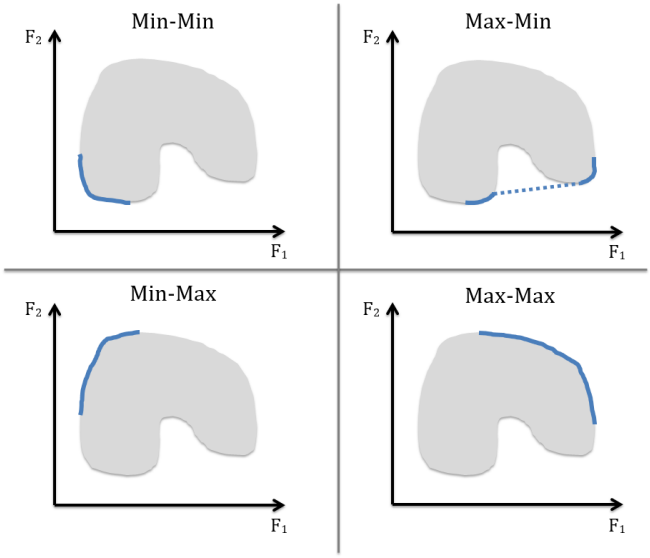

Figure 5. Pareto Fronts for the four combinations of two objectives within the objective space. Figure modeled after [45].

acknowledges the solution could have been found by someone simply looking at the topographical map. However, a computerized search, specifically one done by a classical optimization, would have had extreme difficulty with the problem due to the inordinate local maximums [44].

Genetic programs have been shown to have many advantages over classical optimization methods to include [44]:

- Optimizes over continuous or discrete variables
- Objectives do not have to be differentiable
- Searches simultaneously across the entirety of a wide solution space
- Can handle large numbers of variables
- Can be parallelized
- Can handle variables with complex cost surfaces
- Produces an optimal solution set versus a single solution

There are as many different types of GPs as there are applications of GPs and within each type there are various configurations leading to a near limitless possibility of "unique" GPs. A few current GPs are listed in Table 1 [48].

Table 1. Some current Genetic Programs.

Genetic Programs
neighborhood cultivation genetic algorithm (NCGA)
neighborhood constraint method (NCM)
niched Pareto genetic algorithm (NPGA)
niched Pareto genetic algorithm 2 (NPGA2)
non-dominated sorting differential evolution (NSDE)
non-dominated sorting genetic algorithm (NSGA)
non-dominated sorting genetic algorithm II (NSGA-II)
non-dominated sorting memetic algorithm (NSMA)
non-inferior surface tracing evolutionary algorithm (NSTEA)
orthogonal multi-objective evolutionary algorithm (OMOEA)
orthogonal multi-objective evolutionary algorithm II (OMOEA-II)
Pareto converging genetic algorithm (PCGA)
parallel multi-objective algorithm (PMOGA)
parallel evolutionary multiobjective optimization-
using hypergraphs evolutionary algorithm (PMOHYPEA)

Of the GAs listed in Table 1, we will use a NSGA-II type algorithm. The NSGA-II algorithm is a fast elitist GA for solving non-convex, non-continuous multiobjective optimizations. NSGA-II algorithm improves upon other non-dominated sorting multi-objective genetic programs, which are criticized because of their computational complexity, non-elitism approach and the need to define a shared parameter [49]. The computational complexity of NSGA-II is MN^2 where M is the number of objectives and N is the population size [49]. The NSGA-II was chosen because of the ease of acquiring and the adaptability allowed for in Matlab's® *gamultiobj* function

implementation of NSGA-II.

2.4 Bi-static synthetic aperture radar (SAR)

Bi-static radar is similar to mono-static radar with the main difference being the dependence of modeling and processing upon the geometry of the scene. Figure 6 shows the defined geometry of a general bi-static radar scene where R_r and R_t are range from scene center to receiver and transmitter, β is the bi-static angle, ϕ_r and ϕ_t are receiver and transmitter azimuth angles, with θ_r and θ_t receiver and transmitter elevation angles. For the general bi-static radar scene, crossrange resolution defined by [50] is

$$\rho_{u_{bi}}^{\perp} = \frac{c}{4f_r \sin\frac{\Delta\phi_r}{2}\cos(\theta_r)\cos(\beta/2)} \qquad \text{where } \beta = \arccos\left(\frac{\mathbf{r} \bullet \mathbf{t_j}}{\|\mathbf{r}\| \ \|\mathbf{t_j}\|}\right) \tag{3}$$

where c is the speed of light, $\Delta\phi_r$ is the azimuth extent of the receiver, θ_r the receiver elevation, β is the bi-static angle between the receiver and transmitter. The receiver position vector is $\mathbf{r} = (x_r, y_r, z_r)$, and $\mathbf{t_j} = (x_{t_j}, y_{t_j}, z_{t_j})$ is the transmitter position vector in meters.

Bi-static range resolution is defined by [50] as

$$\rho_u = \frac{c}{2B_j\cos(\beta/2)} \tag{4}$$

where B_j is the bandwidth common to the receiver and jth transmitter.

With $\lambda_r = \frac{c}{f_r}$, the bi-static signal to noise ratio (BSNR) is defined as [50]

$$\text{SNR}_{bi} = \frac{c^2 P_{t_j} G_{t_j} G_r \sigma_j}{f_r^2 (4\pi)^3 R_{t_j}^2 R_r^2 k T_0 F_r B_r}. \tag{5}$$

where subscript j is the jth transmitter, P_t is transmitter power, G_t and G_r are linear transmitter and receiver antenna gains, λ_r is ideal wavelength of the receiver center frequency, and σ_j is the bi-static cross-section of the scatter relative to the receiver and jth transmitter pair. R_t is the range from transmitter to scene center, R_r the range from receiver to scene center, k is Boltzmann's constant, T_0 is 290°K, with F_r and B_r the linear noise figure and filtered bandwidth of the receiver respectively.

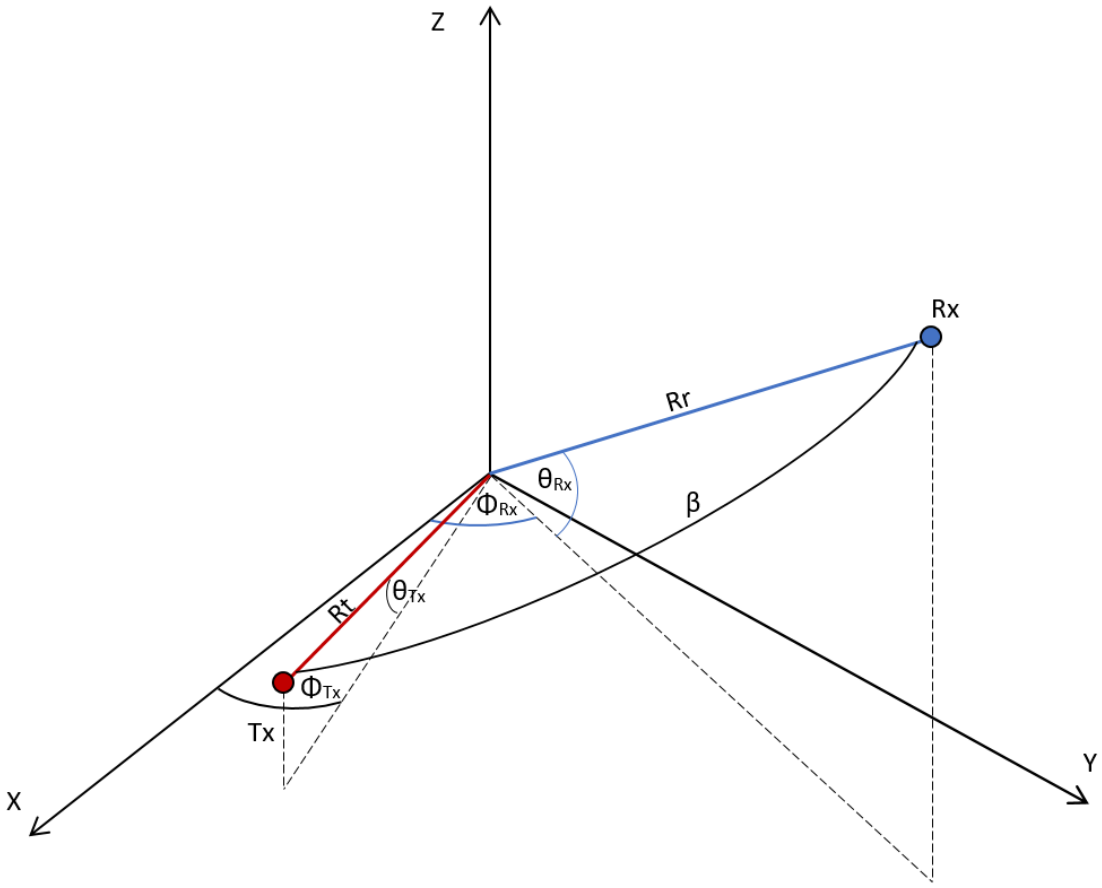

Figure 6. Geometry of a bi-static scene.

III. Methodology

In this chapter we define a specific multi-objective optimization (MOO) model patterned after the general form discussed in Chapter I. The methods used to solve the multi-objective optimization (MOO) through implementation of Matlab's® *ga-multiobj* function are also described.

3.1 Optimization

The receiver optimization problem incorporates many objectives: good resolution, strong signal, adequate frequency space coverage, as well as multiple constraints imposed due to transmitter parameters and receiver limitations. Stevens [9] made an exhaustive search model for a multi-static system where all parameters were known. Receiver parameters did not contribute to the combinations of the search within Stevens' model. Our model allows the configuration of receiver parameters to optimize across transmitter pairings. Expanding upon the general MOO model presented in Equation (1) of Chapter I, we define a general receiver optimization model as

$$\boldsymbol{\gamma}_{opt} = \left\{ \begin{array}{ll} \underset{\gamma\in[R_r,\phi_r,\theta_r,f_r]}{\text{argmax}} & \text{SNR}_{bi}(f_r, R_r, R_{t_j})\text{Ind}(f_r, f_{t_j}) \\ \underset{\gamma\in[R_r,\phi_r,\theta_r,f_r]}{\text{argmin}} & \rho_u^{\perp}\big(f_r, \beta(\phi_r, \theta_r, \phi_{t_j}, \theta_{t_j})\big)\text{Ind}(f_r, f_{t_j}) \\ \underset{\gamma\in[R_r,\phi_r,\theta_r,f_r]}{\text{argmin}} & \rho_u\big(\beta(\phi_r, \theta_r, \phi_{t_j}, \theta_{t_j})\big)\text{Ind}(f_r, f_{t_j}) \end{array} \right. \quad \mathbf{s.t.} \quad \begin{array}{l} R_r \in [R_{r_{min}}, R_{r_{max}}] \\ \phi_r \in [\phi_{r_{min}}, \phi_{r_{max}}] \\ \Delta\phi_r = a^{\circ} \\ \theta_r \in [\theta_{r_{min}}, \theta_{r_{max}}] \\ f_r \in \{f_{t_1}, \ldots, f_{t_{N_T}}\} \end{array} \tag{6}$$

where $\text{Ind}(f_r, f_{t_j})$ is an indicator function defined as

$$\text{Ind}(f_r, f_{t_j}) = \left\{ \begin{array}{ll} 1 & \text{if } f_r = f_{t_j} \\ \emptyset & \text{else} \end{array} \right\}$$

so that each objective is evaluated using the jth transmitter parameters $[R_{t_j}, \phi_{t_j}, \theta_{t_j}, f_{t_j}]$ if $f_r = f_{t_j}$.

The range of receiver frequencies is constrained to the set of transmitter frequencies, since it is impractical to have a receiver operate outside of an available transmitted frequency. Choosing $f_r = f_{t_j}$ determines the paired transmitter, and all parameters associated with the jth transmitter are now carried into metrics which require any transmitter parameter. The problem formulation as modeled in (6) is easily extended to the multi-static case by simply defining and using multi-static objective functions and multiple transmitters and/or receivers.

In this work, we study a simplified receiver optimization that tunes only recevier frequency and azimuth location. Thus, we study the optimiztaion problem

$$\boldsymbol{\gamma}_{opt} = \begin{cases} \underset{\gamma\in[\phi_r,f_r]}{\text{argmax}} & \text{SNR}_{bi}(f_r)\text{Ind}(f_r, f_{t_j}) \\ \underset{\gamma\in[\phi_r,f_r]}{\text{argmin}} & \rho_u^{\perp}\big(f_r, \beta(\phi_r, \phi_{t_j})\big)\text{Ind}(f_r, f_{t_j}) \\ \underset{\gamma\in[\phi_r,f_r]}{\text{argmin}} & \rho_u\big(\beta(\phi_r, \phi_{t_j},)\big)\text{Ind}(f_r, f_{t_j}) \end{cases} \quad \textbf{s.t.} \quad \begin{array}{l} R_r = 12,000 \\ \phi_r \in [0, 2\pi) \\ \Delta\phi_r = \frac{30\pi}{180} \\ \theta_r = \frac{30\pi}{180} \\ f_r \in \{f_{t_1}, \ldots, f_{t_{N_T}}\}. \end{array} \tag{7}$$

To illustrate the impact of transmitter selection upon receiver design, let's look at the first metric in the MOO (7), SNR_{bi}. If a bi-static pairing of Receiver 1 and Transmitter 5 were selected, calculating the BSNR as defined in (5) would not only select the receiver center frequency to equal the transmitter center frequency, it would also populate the equation with the power (P_{t_j}), gain (G_{t_j}) and range (R_{t_j}) of the chosen jth transmitter. Thus any transmitter parameter is a function of or dependent upon f_r from the MOO's perspective, since choosing $f_r = f_{t_j}$ locks in the subsequent

geometries and parameters inherent to the jth transmitter.

With both BSNR (5) and bi-static crossrange resolution (3) dependent upon the inverse of signal frequency, $\frac{1}{f_r}$, increasing the frequency will reduce both BSNR and crossrange resolution. However, since it is the goal of the optimization to maximize BSNR and minimize crossrange resolution (7), these two objectives compete against each other and the trade space between them must be established by the decision maker.

A genetic algorithm is used to perform the receiver design optimization described in (7), due to the complexity of the optimization. The complexity comes from the optimization being a constrained, multi-objective, combinatorial problem, with both discrete and continuous parameters and variables. [45, 49, 51, 52]. Matlab's® *gamulti-obj* function is one genetic algorithm multi-objective optimization (GAMOO) adaptable for multiple constraints upon multiple, mixed variables across multiple objective functions.

Matlab's® *gamultiobj* works across the specified or constrained sample space of the problem. The *gamultiobj* pulls a "sample" population from the defined constraints and algorithm parameters at random from a Gaussian distribution. The algorithm parameters have default values but most can be set by the user to create customizable criteria for algorithm termination, population size, number of generations, as well as mutation and crossover points to name a few.

Once the initial population is drawn, the objective functions are then applied to the selected population, a subset of the variable domains. The next population or

variable values are chosen using the non-dominated rank and distance measure of the individuals in the current population. If one individual, a, in a population has a higher rank than another, b, a is dominant to b as described in Section 2.3 and shown in Figure 4. If two individuals are of the same rank, the algorithm uses the distance measure to compare the two. The distance measure is the Euclidean distance from one individual to another of the same rank [53] within the objective space.

Matlab's® *gamultiobj* uses a controlled elitist genetic algorithm which is a variant of NSGA-II [45]. As such, the algorithm prefers individuals within the population space which have a higher rank, but also has a preference for those that increase the diversity of the population. The preference for diversity means the algorithm includes individuals who help increase diversity even if they are lower ranking. The diversity in the population is vital to obtain a convergence upon the Pareto front by avoiding local optima and is controlled in the algorithm using the algorithm's "ParetoFraction" and "DistanceFcn"options. The "ParetoFraction" limits the number in the current population that are on the Pareto front. The "DistanceFcn" maintains population diversity by giving favor to those individuals on the front that are relatively far apart [54]. The default "ParetoFraction" is 0.35 and the default for "DistanceFcn" is to measure the distance in the objective or function space [53].

The *gamultiobj* function requires a minimum of two declared inputs: the objective functions and the number of variables. The other possible inputs of linear constraints, equality constraints, upper and lower variable bounds, nonlinear constraints, and "options" can be left blank if none are desired. The input values can all be customized by the user. The "options" input allows for myriad customizations, to include customized creation functions, population initialization, termination require-

ments, mutation functions and crossover points. The "options" input also allows for various parameters to be plotted or displayed. An example of this is the option to plot the Pareto front as the algorithm runs.

Outputs of the *gamultiobj* function include: resulting optimal variable values, corresponding optimal objective values, reason for algorithm termination, state of the random number generator before algorithm started, total number of generations, total number of function evaluations, maximum constraint violation, final population values as well as the ranks of final population to name a few.

The objectives are defined in Matlab as functions which allow for vectored variables $\mathbf{x} = [x(1), x(2) \ldots, x(numvar)]$, where numvar is the number of variables. The multiple objective functions are then concatenated into one "fitness function" for the *gamultiobj* algorithm. By customizing mutation and crossover functions of the algorithm, Matlab's® *gamultiobj* can be configured to operate on discrete or continuous variable, also called "mixed variable" problems. Custom mutation functions and crossover functions were required because of the mixed nature of our model (7). Customized mutation and crossover functions, allow the user to declare which variables are discrete as well as to ensure that any subsequent mutation and mating of parents results in a discrete offspring. In our case, this allowed for frequency selections from the set of specified frequencies corresponding to the transmitter frequencies. The customized mutation and crossover functions accomplished discrete offspring by forcing any resulting child to an integer value within the constrained variable set. In our custom crossover and mutation functions we round to the nearest viable integer value.

With the discrete integer values declared in the upper and lower bounds of the

frequency variable, it was necessary to map the frequency integer obtained by the algorithm to the corresponding transmitter frequency. Mapping was accomplished by customizing the objective functions to use the integer value passed by the algorithm population results to reference the appropriate transmitter frequencies. The customized mapping of the the integer to the corresponding transmitter also mapped other transmitter parameters such as location. As with the MOO model defined in (7), implementation of the model into *gamultiobj* function can be easily expanded to multi-static scenarios with mixed variables by simply defining the respective multi-static objectives.

3.2 Bi-static synthetic aperture radar (SAR)

Generated SAR images of a predefined scene are used to illustrate the effectiveness of the receiver design optimization, by analyzing the resulting image quality as defined by the metrics of the MOO in Equation (7). Images for pairings identified as optimal for bi-static imaging by the GAMOO are compared against themselves to evaluate the trade space. All SAR images generated are accomplished using the back-projection algorithm [55]. It is assumed that the phase history of the scene was perfectly captured by the matched filter and, thus, no degradation of the reflected signal occurred. It is also assumed that all sampling was above the Nyquist sampling rate required so no aliasing occurred due to sampling deficiencies [56].

IV. Results

This chapter examines the results of Matlab's® *gamultiobj* implementation of the MOO and examines the computational efficiency of the selected genetic algorithm multi-objective optimization (GAMOO) against an exhaustive search model. SAR images of a simple scene are used to show the trade space for image quality identified by the GAMOO Pareto front.

4.1 Scenario

For all results the same general scenario was used with a receiver placed at 12000 meters from scene center whose azimuth angle could range from $[0, 2\pi)$. All transmitters in the scene were placed at a range of 8000.1 meters and whose azimuth angles were linearly spaced across the interval $[0, 2\pi)$. There are N_T transmitters equally spaced in azimuth. The first scenario uses 5 transmitters as shown in Figure 7. Azimuth angle and frequency were the only parameters that varied from transmitter to transmitter. Those parameters which remained constant across all scenarios for both transmitter and receiver are shown in Table 2. The radar cross section for all scatterers in the field is 1 dB/m^2.

The frequency range used for all simulated scenarios is defined by the interval [87.56 MHz, 4.0 GHz]. This frequency range was chosen because of the large concentrations of available signals for use by a passive radar receiver in an urban environment. This range incorporates the International Telecommunication Union (ITU) defined very high frequency (VHF), ultra high frequency (UHF) and the Institute of Electrical and Electronics Engineers (IEEE) defined S band. The set of defined transmitter frequencies is linearly spaced between the interval [87.56 MHz, 4.0 GHz],

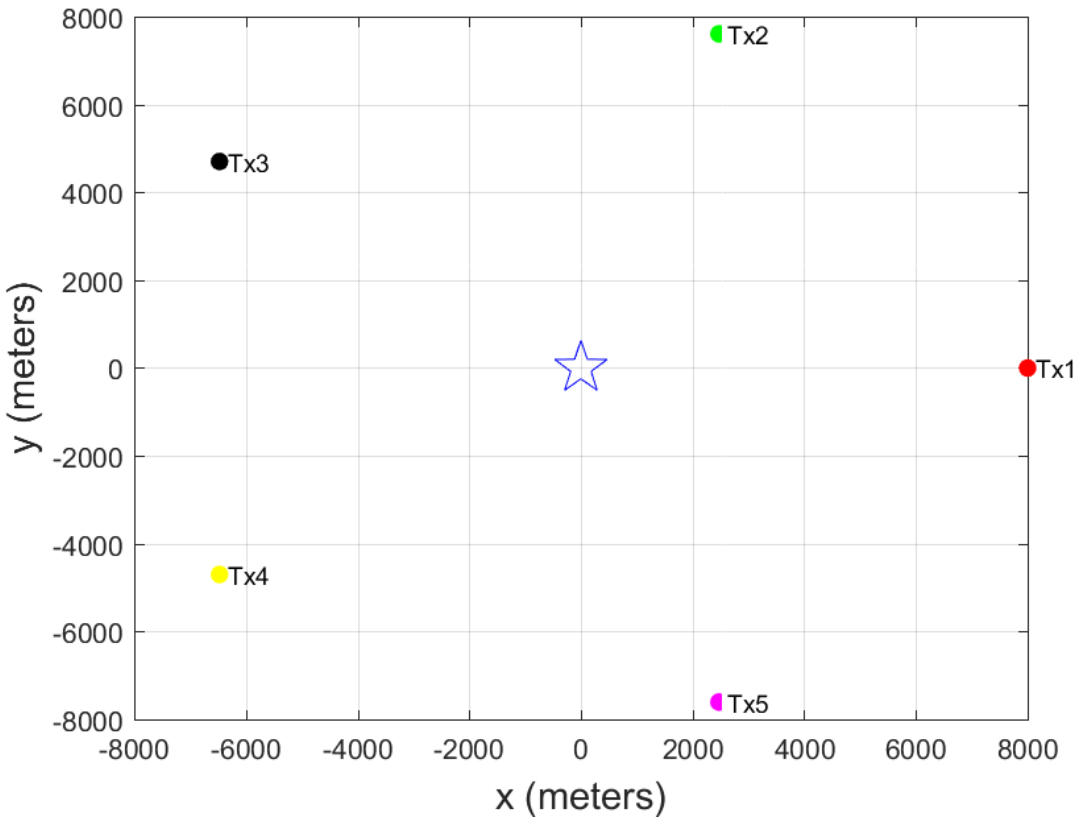

Figure 7. Basic scene scenario with 5 transmitters.

Table 2. Parameters common to all scenarios.

Parameter	Symbol	Value
Transmit Power	P_t	25 kW
Transmit Antenna Gain	G_t	36 dB
Transmitter Elevation	θ_t	$2\pi/180$
Transmitter Range	R_t	8000.1 m
Receiver Antenna Gain	G_r	36 dB
Receiver Elevation	θ_r	$30\pi/180$
Receiver Range	R_r	12000 m
Receiver Azimuth extent	$\Delta\phi_r$	$30\pi/180$
Receiver Bandwidth	B_r	160 MHz
Receiver Noise Figure	F_r	3.2 dB

as listed in Table 3, for N_T transmitters with $N_T \in [1, 20, 50]$.

Table 3. Frequencies for sets of 5, 20 and 50 transmitters with corresponding step values and calculated SNR.

5 Frequencies		**Steps of:**	**978.1100 MHz**	
87.56 MHz	1065.67 MHz	2043.78 MHz	3021.89 MHz	4000 MHz
13.8486 dB	16.2842 dB	19.6811 dB	25.3374 dB	47.0437 dB
20 Frequencies		**Steps of:**	**205.9179 MHz**	
87.56 MHz	293.48 MHz	...	3794.08 MHz	4000 MHz
13.8486 dB	14.3077 dB	...	36.5383 dB	47.0437 dB
50 Frequencies		**Steps of:**	**79.8457 MHz**	
87.56 MHz	167.41 MHz	...	3920.15 MHz	4000 MHz
13.8486 dB	14.0237 dB	...	41.4144 dB	47.0437 dB

Again, it is of particular note that because the defining of the objective functions in the coding is dependent upon pairing choice, picking transmitter 1 subsequently establishes the receiver center frequency to match that of transmitter 1. Further more, the pairing choice then populates all objective values with the parameters of

the chosen transmitter. It is this method of defining the objective functions that allows the optimization to be defined as truly a receiver design optimization. It is also this interdependency on pairing choice that makes holding all transmitter values constant, besides frequency and azimuth angle, necessary for this research. Calculated SNR values are relatively high based upon the parameter settings chosen. However, since the goal of this research was to examine the effectiveness and efficiency of a GA to solve the multi-objecitve optimization, unrealistically high SNR values did not impact this work. If examining the trade space provided by the GA relative to real-world, more true to life SNR values would need to be obtained through appropriate platform parameter settings.

4.2 Exhaustive Search

To begin with, a subset of the MOO (7) was implemented using two of the three objectives (BSNR and crossrange resolution) to more easily express and interpret the resulting Pareto front values. As shown in Table 2, the bandwidth common to each transmitter/receiver pair was held constant in the model, so optimizing crossrange resolution also results in optimized range resolution in this case. The two objective model programmed in Matlab was

$$\boldsymbol{\gamma}_{opt} = \begin{cases} \underset{\gamma\in[\phi_r,f_r]}{\text{argmax}} & \text{SNR}_{bi}(f_r)\text{Ind}(f_r, f_{t_j}) \\ \underset{\gamma\in[\phi_r,f_r]}{\text{argmin}} & \rho_u^{\perp}\big(f_r, \beta(\phi_r, \phi_{t_j})\big)\text{Ind}(f_r, f_{t_j}) \end{cases} \quad \mathbf{s.t.} \quad \begin{aligned} & R_r = 12,000 \\ & \phi_r \in [0, 2\pi) \\ & \Delta\phi_r = \tfrac{30\pi}{180} \\ & \theta_r = \tfrac{30\pi}{180} \\ & f_r \in \{f_{t_1}, \ldots, f_{t_{N_T}}\} \end{aligned} \tag{8}$$

To fully describe the entire trade space defined by the two objectives of BSNR

and cross range resolution, an exhaustive search is accomplished. The exhaustive search is conducted for all feasible bi-static pairs across two variables: receiver frequency (f_r) and receiver azimuth (ϕ_r) for five transmitters as depicted in Figure 7. The discrete range of receiver frequencies matches available transmitter frequencies of $f_t, f_r \in \{87.56$ MHz, 1.0657 GHz, 2.0438 GHz, 3.0219 GHz, 4.000 GHz $\}$. Receiver azimuth has an integer discrete value range $\phi_r \in [0, 2\pi)$ as discussed above in Section 4.1. While the domain of receiver azimuth is in theory wholly continuous, the discretization for the simulation is integer. Searching the entire design space of the two objectives across the two variables allows us to definitively find the optimization of the two objectives, or to perfectly describe the Pareto front for the discrete space. With the variable domain of receiver frequency and receiver center azimuth defined above and having two objectives, $5 \times 360 \times 2 = 3600$ objective function calculations are required to complete the exhaustive search, ignoring any subsequent "lower level" or nested calculations needed within the objective equations themselves.

The image plot of the crossrange resolution as a function of frequency (f_r) and receiver azimuth (ϕ_r) is shown in Figure 8. As expected from Equation (3) there is a non-linear rise in crossrange resolution value as frequency decreases. The values are clipped on the image plot at 12 m to more fully display the behavior of crossrange resolution at the lower values. The main peak of 25 m at π or 180° makes sense since this occurs at the lowest frequency, which corresponds to Tx_1 whose azimuth is 0. Looking at the equation for crossrange resolution (3) we can see if the frequency is held constant, the bi-static angle becomes the only varying value as receiver azimuth changes. With $\cos(\beta/2)$ in the denominator, crossrange resolution will have its greatest value when the bi-static angle is 180°. With transmitter azimuth changing for each transmitter, the anomalies appearing off the main peak of the crossrange reso-

lution plot are explained by examining the bi-static angle as a function of frequency and receiver azimuth.

The dependence of bi-static angle (β) upon receiver frequency (f_r) and receiver azimuth (ϕ_r) is displayed in Figure 9. Receiver azimuth (ϕ_r) affects receiver location, and thus the bi-static angle. The bi-static angle contributes to crossrange resolution through the ratio of $\frac{1}{\cos(\beta/2)}$ as discussed above and shown in (3). The ratio accounts for the anomalies that are inconspicuous in the crossrange resolution surface plot. The anomalies are due to the fact that each of the five transmitters are at different locations. As the receiver frequency is changed, the transmitter/receiver pairing is changed. Moving from one transmitter to another, the resulting bi-static angle is also changed being a function of receiver and transmitter location. For a single frequency, and thus a single transmitter location, the bi-static angle ranges from 0 to π as the receiver azimuth is varied on the interval of [0, 2π]. The bi-static surface becomes a sinusoidal shape along the single frequency cut. With five locations tied to five differing frequencies, the bi-static angle surface becomes a wave of five sinusoidal peaks. The value of the peaks does not range from the expected [0,π] or [$0^\circ, 180^\circ$] but falls $\approx 30^\circ$ short at each end of the interval. The reduced interval of beta values is due to the elevation angles of the platforms and the resulting 3D bi-static angle. The resulting bi-static image pattern can be seen in the crossrange resolution image (compare Figures 8 and 9), but at attenuated values due to the dependence of crossrange resolution upon frequency.

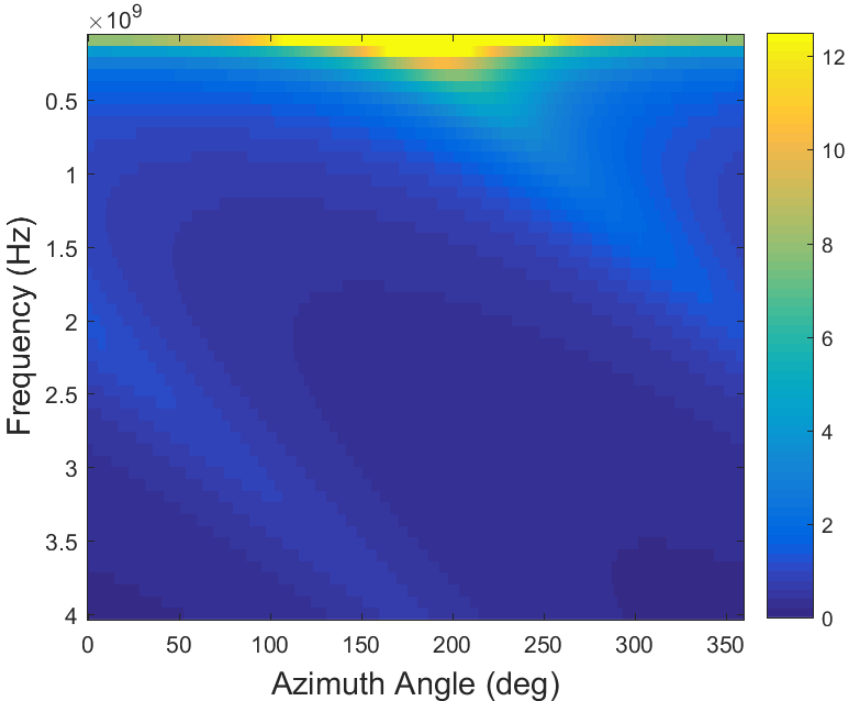

Figure 8. Crossrange resolution image plot across receiver frequency and azimuth.

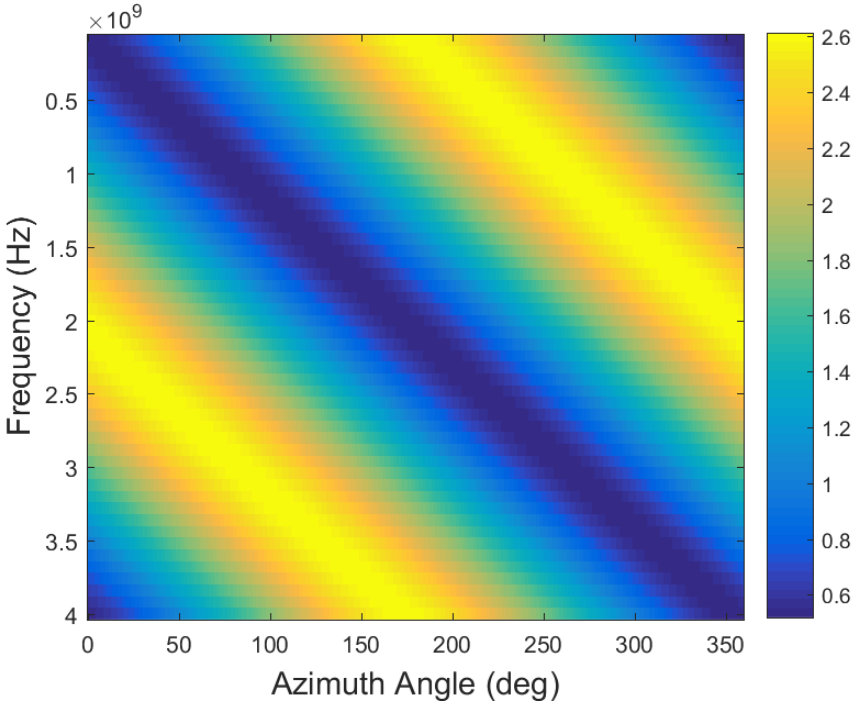

Figure 9. Bistatic angle (β) image plot across receiver frequency and azimuth.

The independence of BSNR upon receiver azimuth (ϕ_r) is shown in Figure 10. The value of BSNR does not change for any one frequency across all azimuths. The inverse relation of BSNR to frequency, $1/f_r^2$ as described in (5), is also displayed in Figure 10.

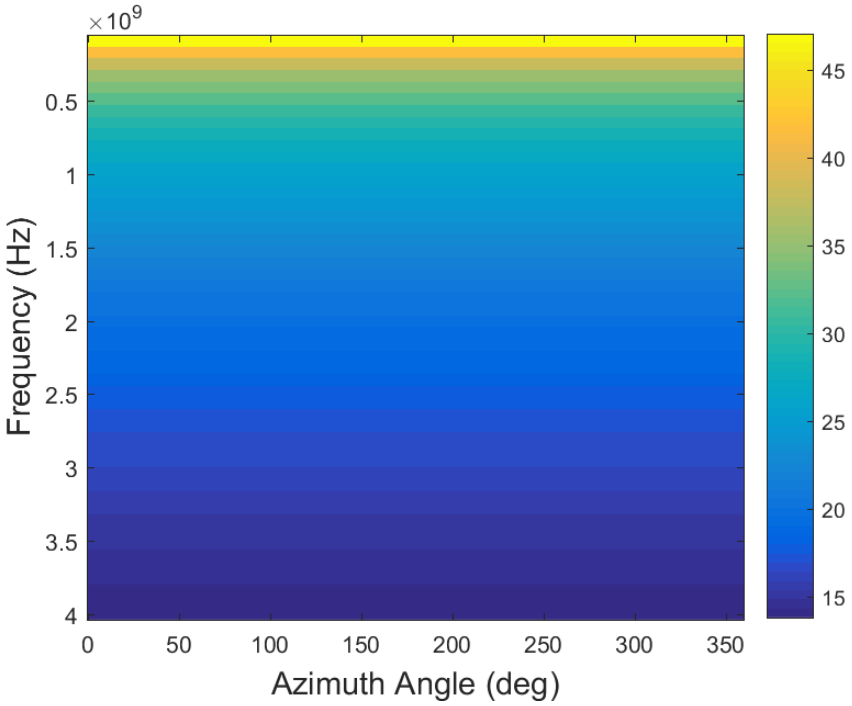

Figure 10. Signal to noise ratio (SNR) image across receiver frequency and azimuth.

Plotting every point obtained from the exhaustive search on the objective axes of SNR and crossrange resolution results in Figure 11. The five frequencies used are shown by the groupings along the SNR axis in Figure 11. The closer proximity of the groupings as you move left on the SNR axis in Figure 11 is due to the $1/f^2$ ratio in the bi-static SNR (5). As f increases, f^2 increases at a non-linear rate thus decreasing SNR non-linearly and crowding to the left of the plot quickly as f increases. All five frequency clusters are discernible with SNR shown in dB scale. At each of the frequency groups, 360 azimuth angle points are shown. The elongation of the groupings across the crossrange resolution shows the increased sensitivity of crossrange resolution to azimuth angle at decreasing frequencies. The increased sensitivity is expected looking at the ratio $\frac{1}{f\cos(\beta/2)}$ defined by (3). With $\cos(\beta/2)$ restricted to (0,1] as the frequency decreases, the effect of the $\cos(\beta/c)$ trending toward zero through a change in azimuth (ϕ_r) has a greater influence to increase the value of the ratio $\frac{1}{f\cos(\beta/2)}$. The

lowest crossrange resolution for each frequency group is indicated by a red triangle in Figure 11 and constitutes the resulting Pareto front of the exhaustive search.

Table 4. Exhaustive Search Pareto Points for 5 Transmitters.

SNR (dB)	CrossRes (m)	Freq (MHz)	RxAzimuth (deg)
13.8486	0.1715	4000.00	288
16.2842	0.2270	3021.89	216
19.6811	0.3357	2043.78	144
25.3374	0.6437	1065.67	72
47.0437	7.8349	87.56	0

Increasing the number of transmitters, and thus frequencies, from 5 to 20, to 50 increases the density of the groupings across the SNR axis, more fully describing the objective space and resulting Pareto front as seen in Figures 12 and 13 respectively. Beyond this increased fidelity within the space, little additional information is obtained regarding the behavior of bi-static SNR and crossrange resolution $\rho_u^{\perp}$, objective functions.

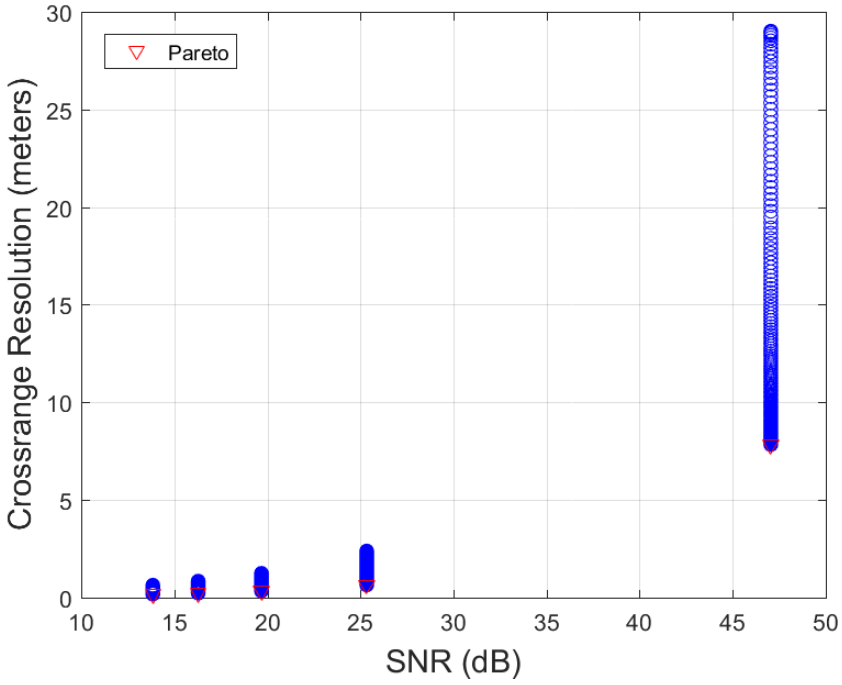

Figure 11. Exhaustive search across 5 transmitters.

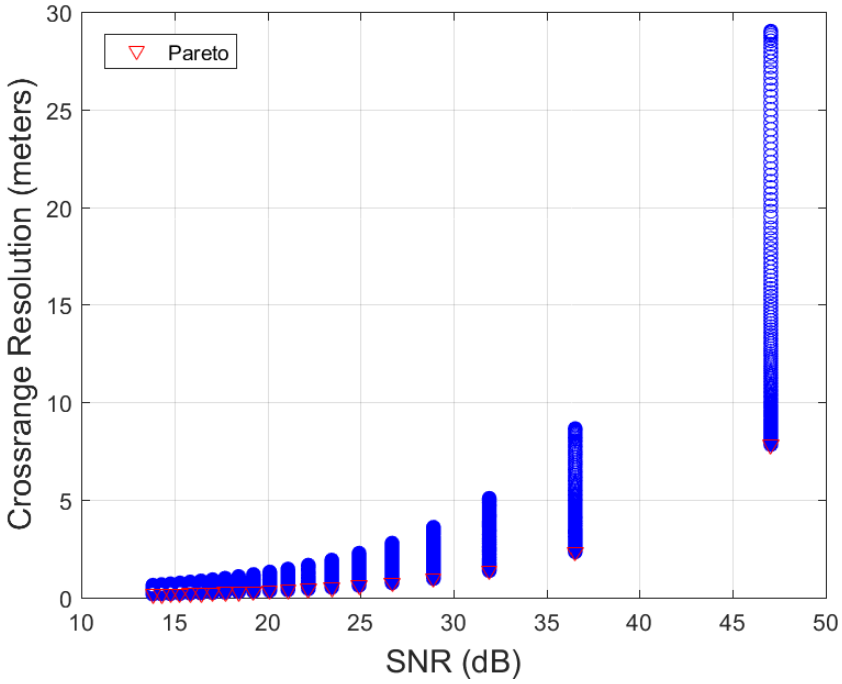

Figure 12. Exhaustive search across 20 transmitters.

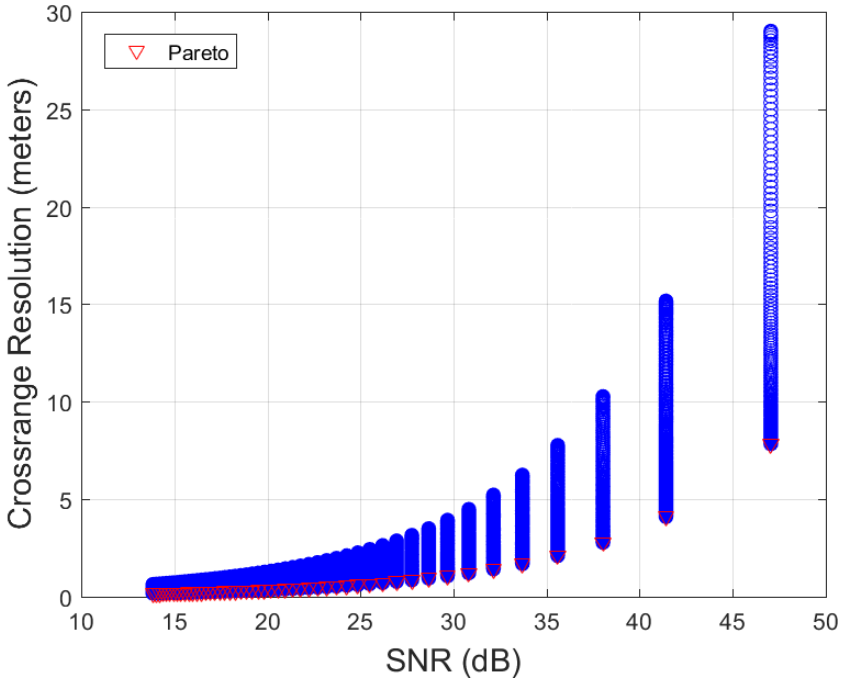

Figure 13. Exhaustive search across 50 transmitters.

4.3 Genetic Algorithm Optimization

While the exhaustive search allows us to perfectly describe the constrained objective space and subsequent Pareto front, it can be quite computationally demanding. For the simple bi-static scenario with five transmitters and an optimization of two objectives across two variables, it required 3600 upper level calculations. The MOO described in (8) was designed and implemented using Matlab's® *gamultiobj* to describe the same trade space found using the exhaustive search in Section 4.2 above. Again the two objectives bi-static SNR and crossrange resolution, are evaluated across two variables: receiver frequency (f_r) and receiver azimuth (ϕ_r).

Running the GA with 5 transmitters produces the plot shown in Figure 14. The objective values as well as the variable values for frequency and receiver azimuth are

displayed in Table 5. The numbers in the left column of Table 5 correspond to the numbered points in Figure 14. It is clearly seen comparing Tables 4 and 5 that the Pareto points obtained by the GA perfectly match those obtained by the exhaustive search from Section 4.2.

Table 5. Objective and variable values obtained by the GA for 5 transmitters.

Point	**SNR (dB)**	**Cross. Res. (m)**	**Freq. (MHz)**	**Rx Azimuth (deg)**
1	13.8486	0.1715	4000.00	288.0000
2	16.2842	0.2270	3021.89	216.0000
3	19.6811	0.3357	2043.78	143.9999
4	25.3374	0.6437	1065.67	72.0007
5	47.0437	7.8349	87.56	0.8183

Figure 14 shows the trade-space available for the maximization of SNR and the minimization of crossrange resolution found by the GA. Because the two objectives have conflicting conditions for optimization, the optimal value for one results in the worst value for the other as expected and shown in the exhaustive search. As described in Section 2.3, each point in Figure 14 is non-dominant.

As with the exhaustive search, the number of transmitters, and thus available frequencies, was increased from 5 to 20, to 50 within the GA. The resulting plots are shown in Figures 15 and 16 respectively. Because the GAMOO algorithm limits the number of points on the front, there is little additional information obtained by increasing the frequency set from 20 to 50 for this scenario, due to the "continuous like" Pareto front defined by the two objectives. Increasing the frequency set would

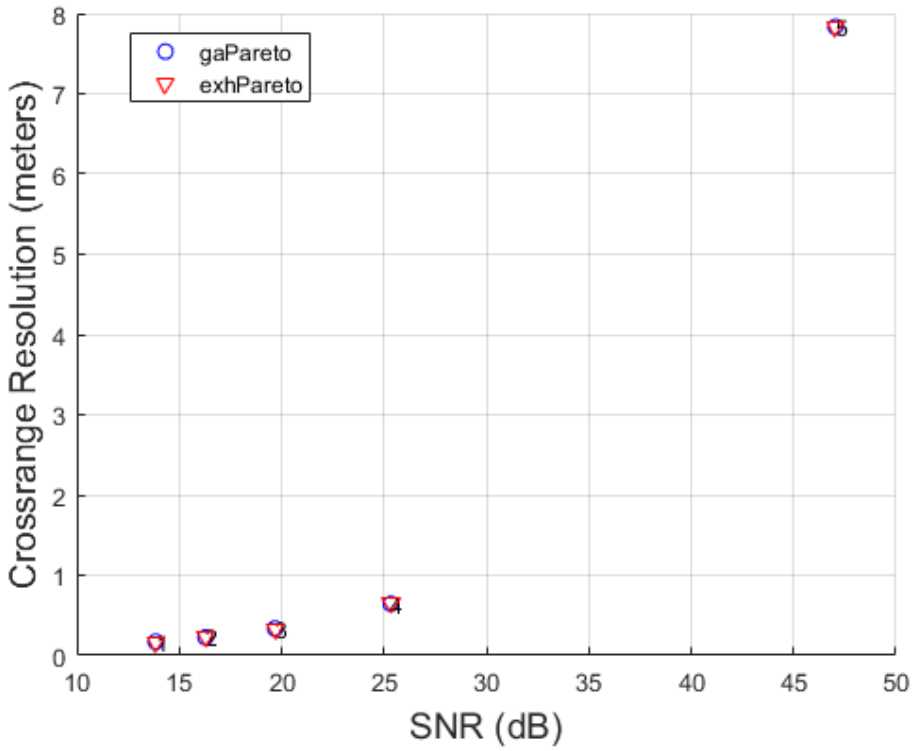

Figure 14. Pareto front obtained by the GA plotted with Pareto front values from exhaustive search for 5 transmitters.

have yielded additional information about the subsequent Pareto front, had there been a discontinuous portion of the front at a frequency within the set of 50 that was not in the set of 20. The values for the 20 and 50 transmitter sets from the GA are shown in Tables 6 and 7. The values for the 20 and 50 transmitter sets are similar to those from the 5 transmitter set shown in Table 5 but provide different spacing in the frequencies selected due to increased set size; 20 and 50 versus 5. Because of the random draw of the initial population, the frequencies for the Pareto points will differ unless a the random number generator is seeded.

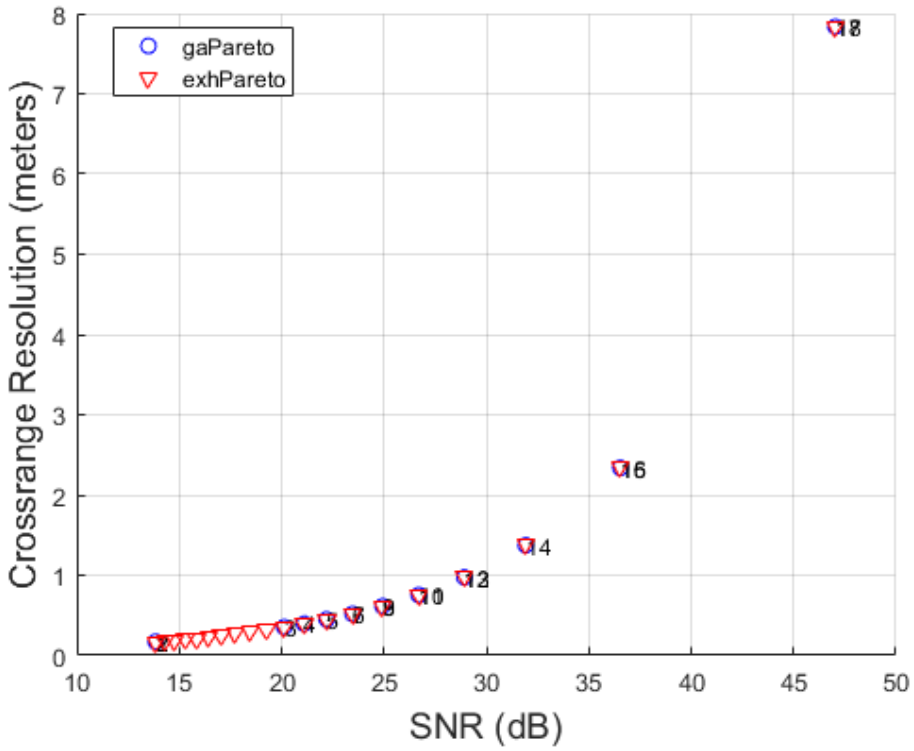

Figure 15. Pareto front obtained by the GA plotted with Pareto front values from exhaustive search for 20 transmitters.

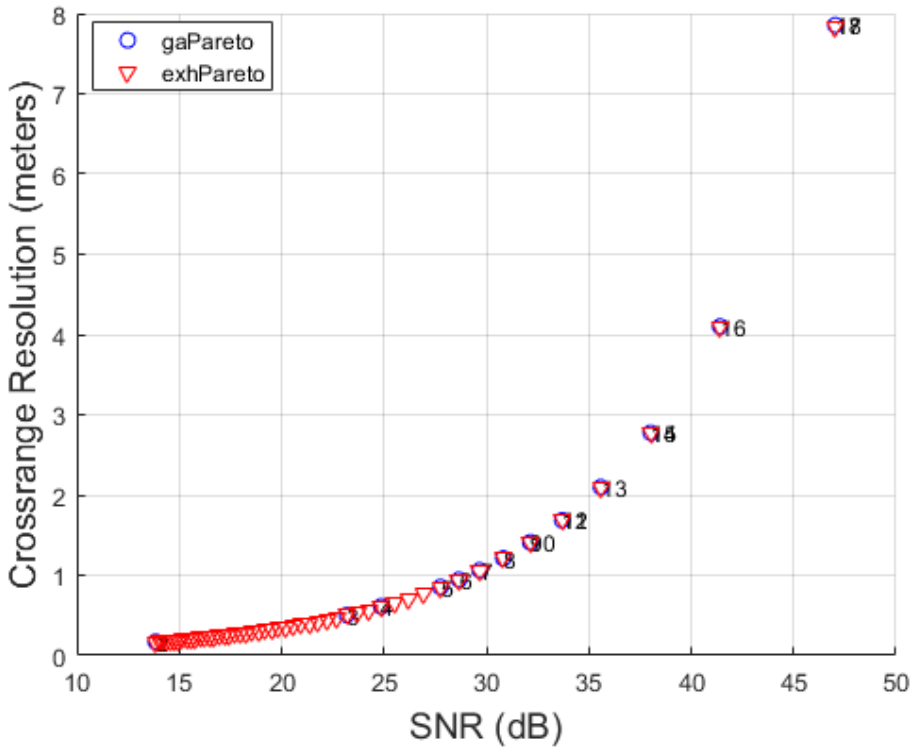

Figure 16. Pareto front obtained by the GA plotted with Pareto front values from exhaustive search for 50 transmitters.

Table 6. Objective and variable values obtained by the GA for 2 objectives across 20 transmitters.

Point	SNR (dB)	Cross. Res. (m)	Freq (MHz)	Rx Azimuth (deg)
1	13.8486	0.1715	4000.0000	340.8162
2	13.8486	0.1715	4000.0000	340.8162
3	19.2542	0.3196	2146.7389	177.4186
4	21.1043	0.3955	1734.9032	146.8206
5	22.2017	0.4487	1528.9853	126.0130
6	23.4582	0.5185	1323.0674	108.1385
7	24.9276	0.6141	1117.1495	90.0020
8	24.9276	0.6141	1117.1495	90.0020
9	26.6972	0.7528	911.2316	71.9651
10	26.6972	0.7528	911.2316	71.9651
11	28.9222	0.9726	705.3137	54.0000
12	28.9222	0.9726	705.3137	54.0000
13	31.9209	1.3737	499.3958	35.9857
14	31.9209	1.3737	499.3958	35.9857
15	36.5383	2.3375	293.4779	18.0000
16	36.5383	2.3375	293.4779	17.9999
17	47.0437	7.8360	87.5600	2.2090
18	47.0437	7.8360	87.5600	2.2090

Table 7. Objective and variable values obtained by the GA for 2 objectives across 50 transmitters.

Point	SNR (dB)	Cross. Res. (m)	Freq. (MHz)	Rx Azimuth (deg)
1	13.8486	0.1716	4000.0000	348.0741
2	13.8486	0.1716	4000.0000	348.0741
3	23.1866	0.5027	1365.0914	112.4657
4	24.8625	0.6111	1125.5543	84.9139
5	27.7613	0.8513	806.1714	68.3998
6	28.6672	0.9445	726.3257	57.5722
7	29.6787	1.0611	646.4800	50.4081
8	30.8238	1.2107	566.6343	43.1199
9	32.1430	1.4092	486.7886	35.9985
10	32.1430	1.4092	486.7886	35.9985
11	33.6991	1.6858	406.9429	28.8000
12	33.6991	1.6858	406.9429	28.8000
13	35.5963	2.0973	327.0971	21.6003
14	38.0270	2.7745	247.2514	14.3926
15	38.0270	2.7745	247.2514	14.3926
16	41.4144	4.0983	167.4057	8.8473
17	47.0437	7.8564	87.5600	8.8473
18	47.0437	7.8564	87.5600	8.8473

The full MOO described in (7) was implemented within the Matlab® *gamultiobj* with the set of 20 transmitters to verify functionality of the algorithm with more than two objectives. The three dimensional objective space for SNR, crossrange

resolution, and range resolution is shown in Figure 17. It appears at first that the Pareto front has an unexpected shape in the range resolution space. This is due to the relatively small scale of the range resolution axis. Because there is such little change in range resolution across the entirety of the space, a receiver azimuth that does not result in a perfect 0 bi-static angle will result in a significantly small difference in range resolution. If the values for range resolution are rounded to the nearest cm, the values become constant at 52 cm. The relative consistency in range resolution across all frequencies is expected, since there were no constraints placed upon receiver azimuth allowing the bi-static angle (β) to always be ≈ 0 and bandwidth was held constant.

Each of the three 2-dimensional Pareto fronts are shown in Figures 18 - 20. As expected the Pareto front in the SNR and crossrange resolution plane, Figure 18, mimics nearly identically the results obtained above for the two objective implementation of the GA, Figure 14. The other 2-dimensional Pareto fronts of SNR/range resoltuion, Figure 19 , and cross range resolution/range resolution, Figure 20, are flat along the range resolution axis when rounding range resolution to the nearest cm as expected (4). Table 8 shows the objective and variable values for the three objective GAMOO whose values are consistent with those in Table 6 for two objectives.

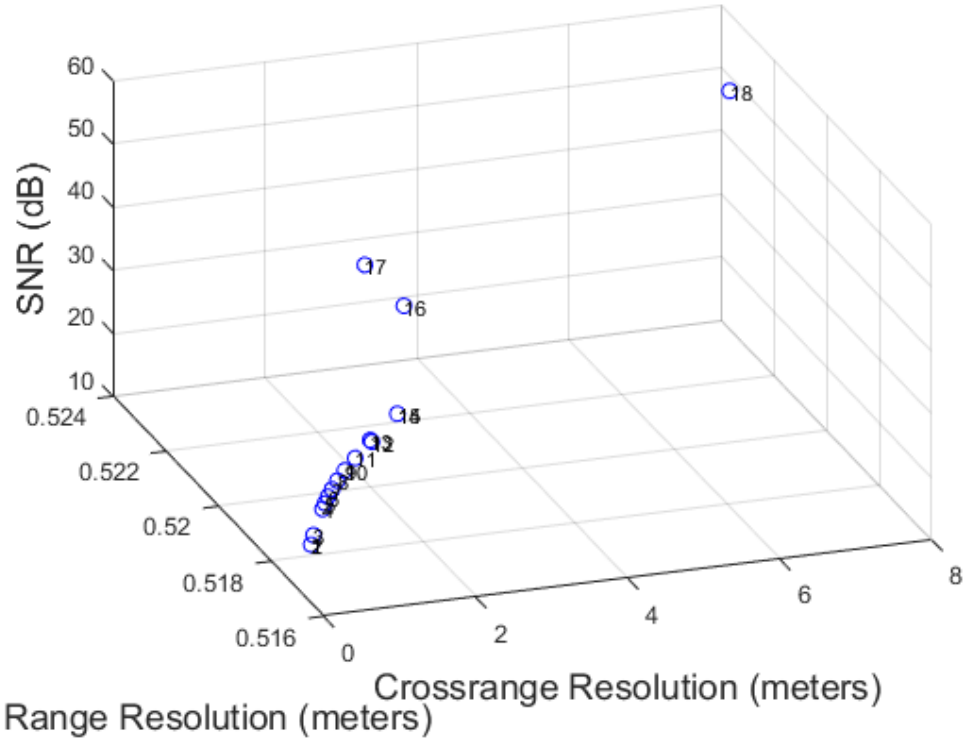

Figure 17. GA Pareto front for 3 objectives: SNR, crossrange resolution, and range resolution for 20 transmitters.

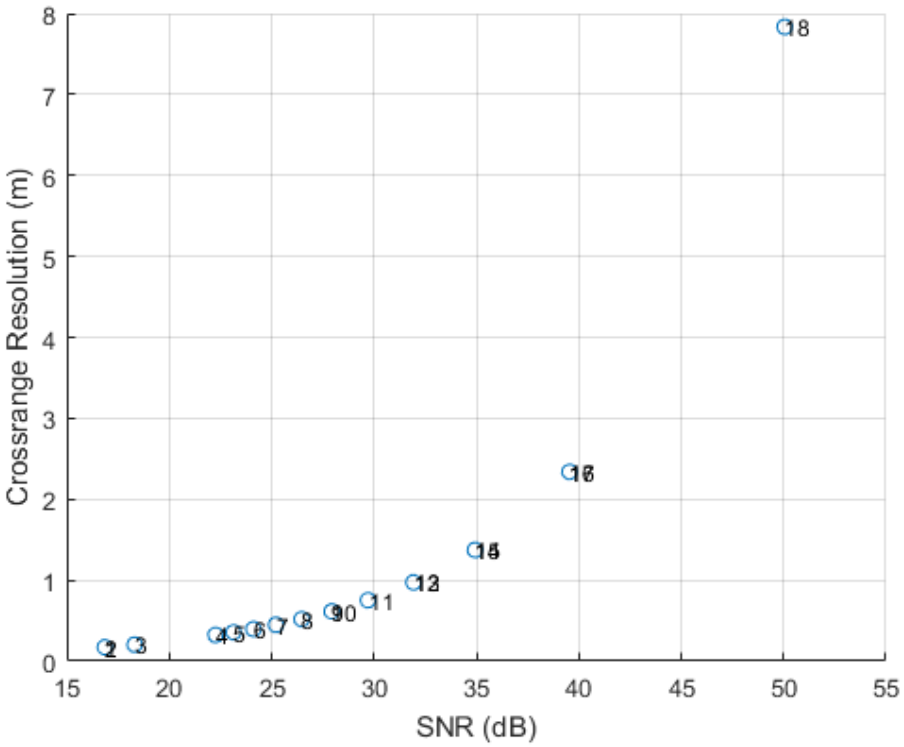

Figure 18. 2 dimensional SNR and crossrange resolution GA Pareto front for 20 transmitters.

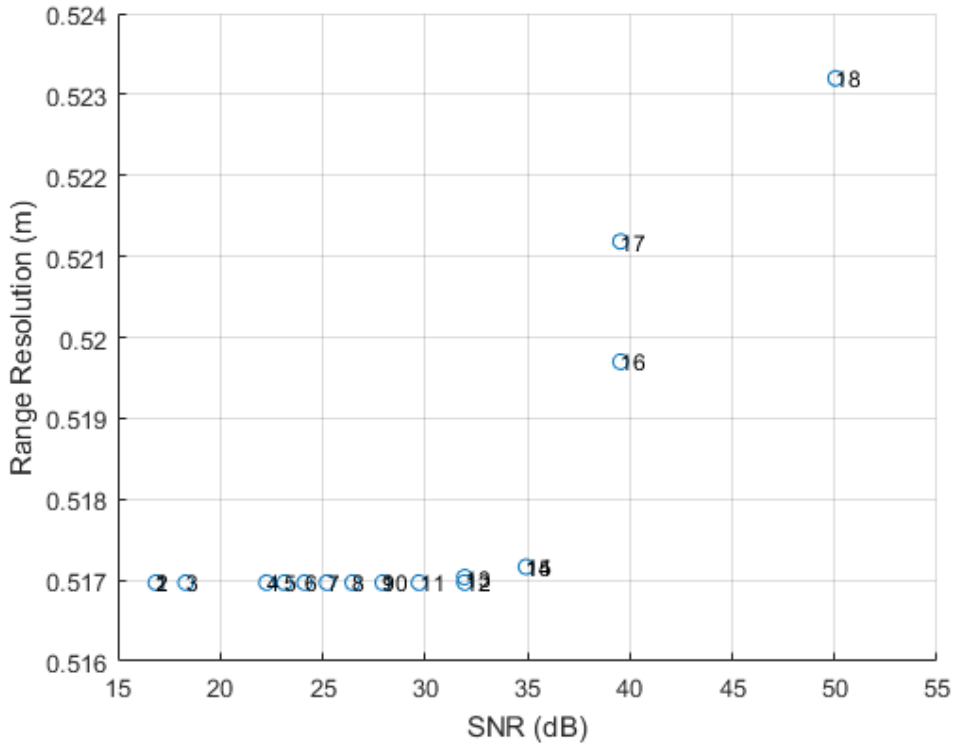

Figure 19. 2 dimensional SNR and range resolution GA Pareto front for 20 transmitters.

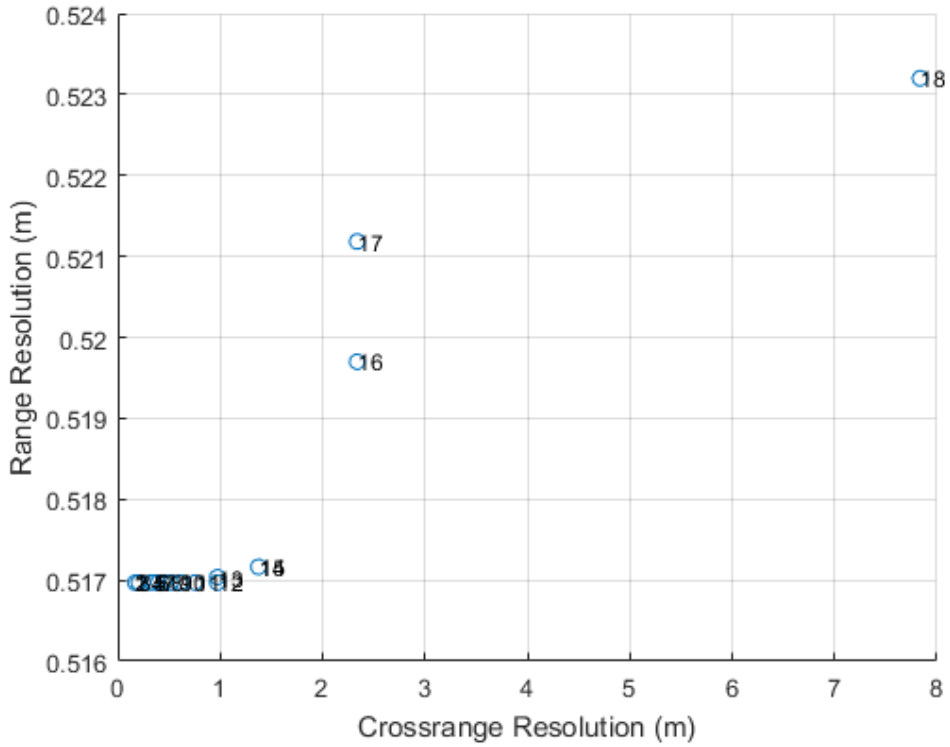

Figure 20. 2 dimensional crossrange and range resolution GA Pareto front for 20 transmitters.

Table 8. Objective and variable values obtained by the GA for 3 objectives across 20 transmitters.

Point	SNR (dB)	Cross. Res. (m)	Range Res. (m)	Freq. (MHz)	Rx Azimuth (deg)
1	13.8589	0.1716	0.5170	4000.0000	338.7331
2	13.8589	0.1716	0.5170	4000.0000	338.7331
3	15.3160	0.2039	0.5170	3382.2463	275.7969
4	19.2645	0.3234	0.5170	2146.7389	161.6093
5	20.1404	0.3563	0.5170	1940.8211	146.8530
6	21.1146	0.3955	0.5170	1734.9032	142.0761
7	22.2120	0.4487	0.5170	1528.9853	125.8533
8	23.4685	0.5185	0.5170	1323.0674	108.0412
9	24.9379	0.6141	0.5170	1117.1495	90.0130
10	24.9379	0.6141	0.5170	1117.1495	90.0130
11	26.7075	0.7528	0.5170	911.2316	72.0212
12	28.9325	0.9726	0.5170	705.3137	53.9996
13	28.9325	0.9726	0.5170	705.3137	53.9996
14	31.9312	1.3737	0.5172	499.3958	35.9934
15	31.9312	1.3737	0.5172	499.3958	35.9934
16	36.5486	2.3375	0.5197	293.4779	17.9919
17	36.5486	2.3375	0.5212	293.4779	17.9919
18	47.0540	7.8347	0.5232	87.5600	0.1038

The Pareto fronts obtained in this Chapter appear smooth for our model of bi-static objectives. Because of the apparent well behaved nature of the Pareto fronts it could be argued that a traditional optimization approach would be appropriate.

However, the point of this research was to show the effectiveness of a GA in solving a general MOO and the flexibility the model has to handle multiple objectives with multiple variables. Keep in mind that our model only varied two variables within the bi-static metrics. Introducing more variable variations as well as more objectives would quickly force the well behaved Pareto fronts into objective spaces with many local optimum and discontinuities. Expanding the model and GA application to multi-static scenarios would exceed the capabilities of traditional optimization methods.

4.4 Computational Complexity

While the Pareto front is shown in greater detail within the exhaustive search when increasing the frequency set, the exponential shape of the Pareto front remains unchanged. The number of objective function calculations required by the exhaustive search jumps from 3600 for 5 frequencies, to 36,000 for 50 frequencies. In contrast, the increasing the frequency set number has no increase of computations within the GAMOO across the sets 5, 20 and 50 frequencies. With the population size of the algorithm set to 50 and the termination conditions set to a function tolerance of $1e^{-4}$, generation limit of 400, and time termination of infinity, the algorithm terminates for all three cases due to function tolerance. The maximum number of computations by the GA was reached with the set of five frequencies, due to the algorithms design to be most efficient with large problems. The set of 5 frequencies required 270 population generations and 11,501 objective computations. The 20 and 50 frequency sets, for both two and three objectives, required 10,151 functional computations across 202 population generations. A side-by-side comparison of the required computations is displayed in Table 9.

Table 9. Number of objective value computations required for the exhaustive search and GA.

Number of Objectives	Number of Transmitters	Exhaustive Search	Genetic Algorithm
2	5	3,600	11,501
2	20	14,400	10,151
2	50	36,000	10,151
3	20	21,600	10,151
3	50	54,000	10,151

The point made by comparing the number of objective value computations is that the information obtained by the GAMOO at each frequency set required roughly the same computations regardless of the variable set size or number of objectives for our problem. It is clear that GAMOO provides the same Pareto Front as the exhaustive search but requires less computations. Our scenario was a simple one but if one were to increased the complexity of the scenario by increasing the variables and/or objectives, the computations necessary for the GAMOO to obtain the Pareto front are quickly dwarfed by the number of computations needed to complete an exhaustive search.

4.5 SAR Image Quality

Images for the transmitter/receiver pairings identified by the GAMOO are generated using the backprojection algorithm. The simple scene used in image generation consists of 43 point scatterers at varying spacing are oriented to spell "AFIT", as shown in Figure 21. The radar cross section of all scatterers was arbitrarily set at 1 dB/m^2. Since all transmitters sets 5, 20, and 50 covered the same frequency interval

of [87.56 MHz, 4.0 GHz] only those from the set of 5 frequencies were evaluated based on the dominate influence of frequency upon resulting objective values. Parameters common to all image generations are shown in Table 10 and meet all Nyquist sampling criteria.

Table 10. Common bi-static SAR image parameters.

Parameter	Value
$\Delta\phi$	$30\pi/180$
Receiver ϕ step size	$0.05/180$
Receiver θ	$30\pi/180$
Transmitter θ	$2\pi/180$
Frequency Bins	1024
Samples in Frequency	2×10^{14}
Common Bandwidth	300 MHz

Figure 22 shows the resulting image from the variable settings of Table 5, Point 1. Point 1 constituted the best crossrange resolution but worst BSNR of all points on the Pareto front. All scatterers are clearly differentiable and the image is fairly clear despite BSNR being the lowest of all points. Figure 23 shows the image resulting from the variable values of Table 5, Point 5. Point 5 had the worst cross range resolution but the highest BSNR of all the points obtained by the GA. It is clear that the crossrange resolution from 0.1715 m to 7.8347 m has a major negative impact upon the image quality. Comparing Figures 22 and 23 it is apparent that while BSNR varied from $\approx$ 13 dB to nearly 50 dB, degradation of BSNR had little impact on image quality. The lack of impact by BSNR upon image quality is due mainly to the assumption of perfect phase history capture. In another scenario where range was increased as well as clutter and noise introduced, BSNR could be expected to play a more influential role in determining image quality.

The image generated using the values of Table 5, Point 3 shows moderate degradation in crossrange resolution as seen in Figure 24. The exponential increase in

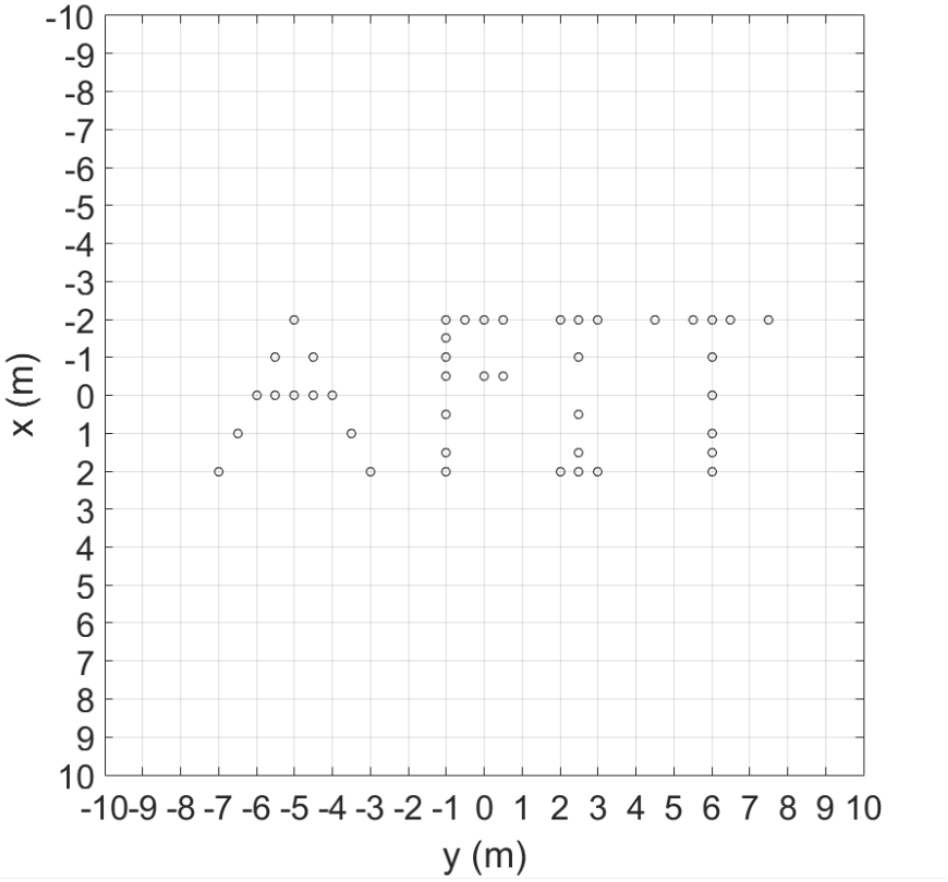

Figure 21. Simple scene layout for bistatic image generation.

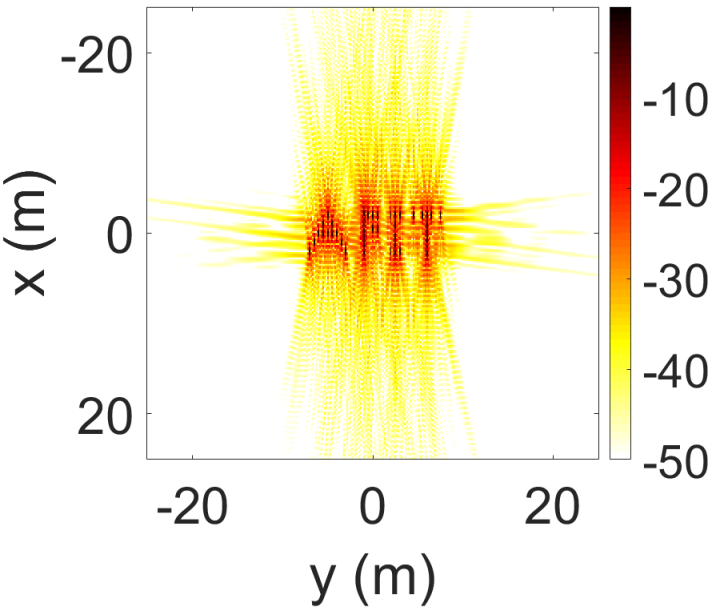

Figure 22. "AFIT" scene SAR image of Table 5, Point 1.

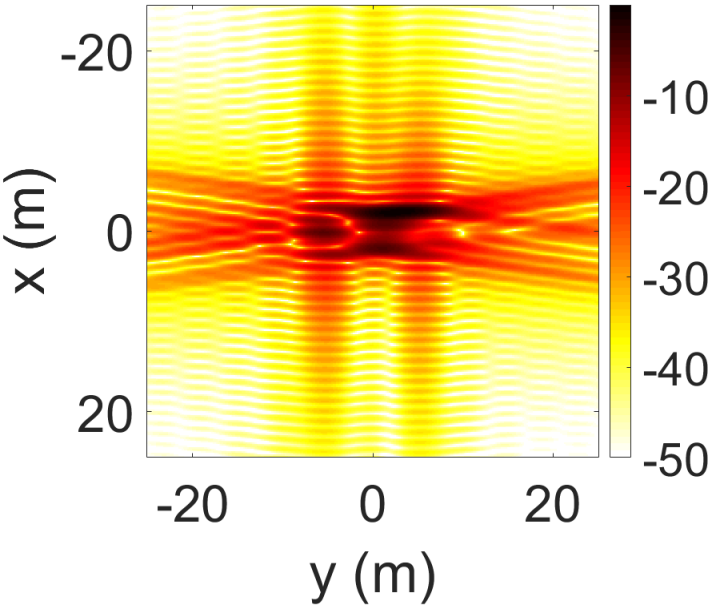

Figure 23. "AFIT" scene SAR image of Table 5, Point 5.

crossrange resolution as frequency increases was shown by the Pareto Front (Figure 14. It would be expected that the degradation in crossrange resolution would be relatively minimal at frequencies ≥ 1 GHz. Comparing the image for values of Table 5, Point 4 in Figure 25 with that of point 5 (Figure 23) we see the expected degradation in crossrange resolution. Table 11 shows the image parameters for all 5 points in Table 5.

Table 11. Bi-static SAR image parameters for 5 Pareto Points in Table 5.

Point	SNR (dB)	Cross. Res. (m)	Range Res. (m)	Freq. (MHz)
1	13.8486	0.1715	0.5170	4000.00
2	16.2842	0.2270	0.5170	3021.89
3	19.6811	0.3357	0.5170	2043.78
4	25.3374	0.6437	0.5170	1065.67
5	47.0437	7.8349	0.5170	87.56

The image generation for Figures 22 - 25 utilized platform parameters that yielded high SNR values with no noise injected into the phase history data. The calculated SNR values are for the center frequency f_r only and approximate the system performance across the sampled bandwidth. In reality, even with a perfectly matched filter, some white Gaussian noise (WGN) would be introduced to the system across all sampled frequencies in the bandwidth. To illustrate the impact WGN has on SAR image quality, we generate images for a scene with a single point scatter at scene center. WGN noise, respective to the frequency of the sampled points, is introduced into the phase history. Figures 26 and 28 show the image quality of the single point scenario with WGN added for Points 1 and 5 in Table 5 respectively. The objective values (SNR and crossrange resolution) are the same as those contained in Table 11. Not much noise is present again due to the high SNR values ($\approx$ 13.8 dB and 47 dB respectfully). However, if we increase the dynamic range to -75 dB, the noise begins to appear as shown in Figures 27 and 29. Decreasing the SNR to nearly 0 dB while

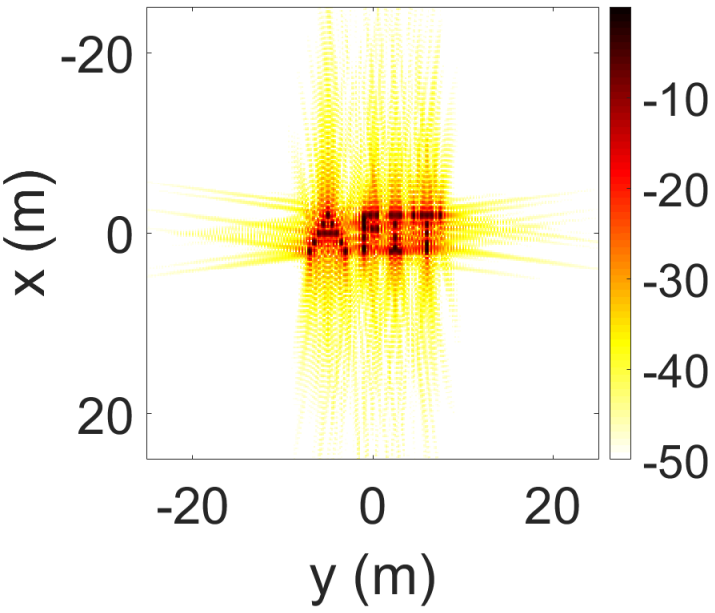

Figure 24. "AFIT" scene SAR image of Table 5, Point 3.

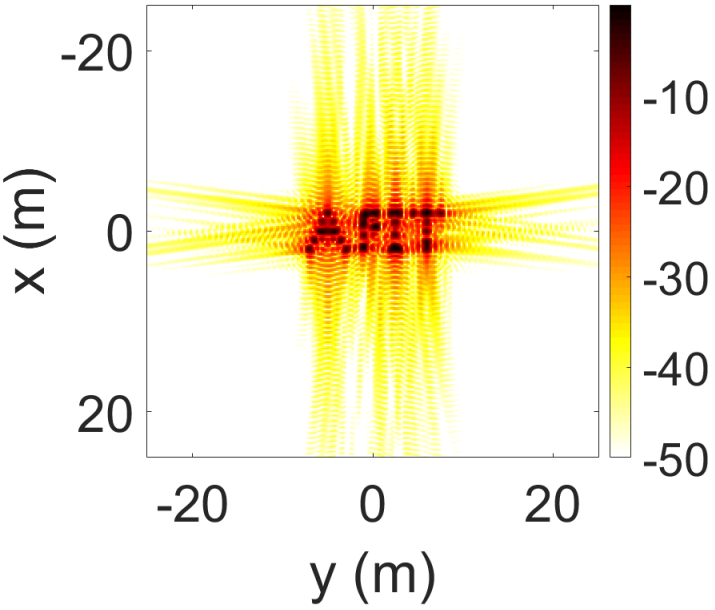

Figure 25. "AFIT" scene SAR image of Table 5, Point 4.

maintaining the same dynamic range enhances the WGN's presence. Figure 30 shows the increased noise influence at a lower SNR.

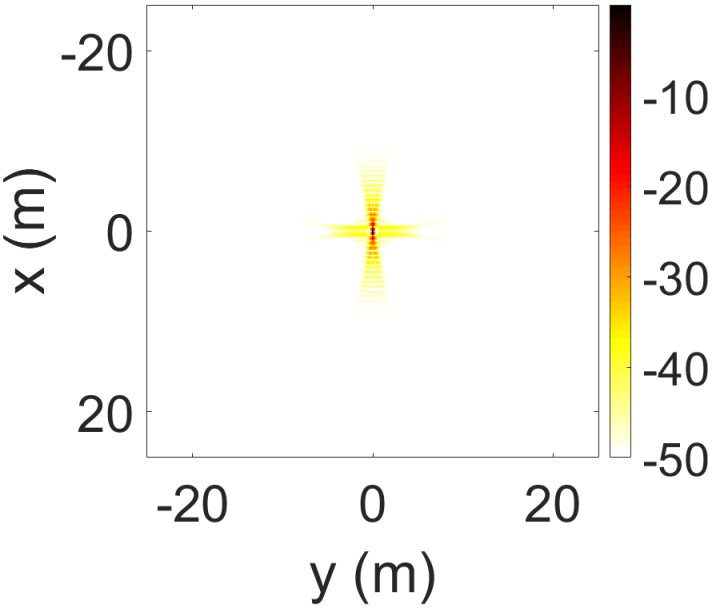

Figure 26. Single point scatter scenario SAR image of Table 5, Point 1 containing noise.

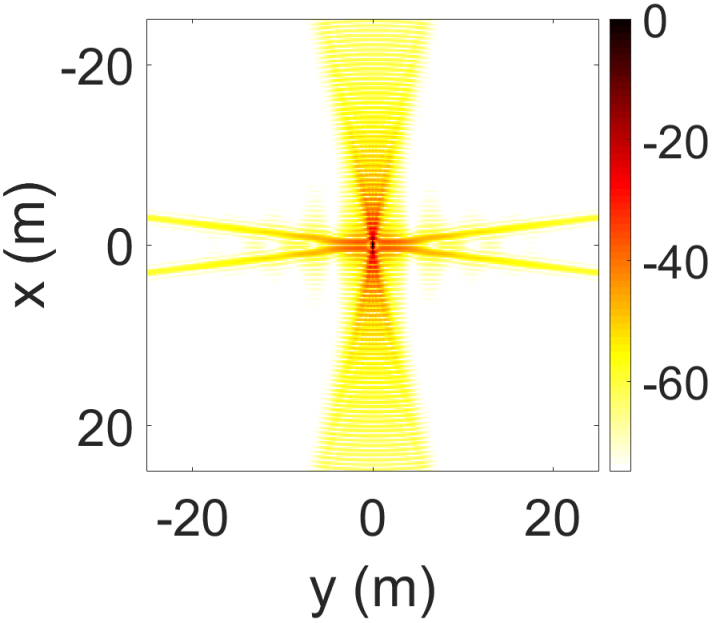

Figure 27. Single point scatter scenario SAR image of Table 5, Point 1 containing noise and increased dynamic range.

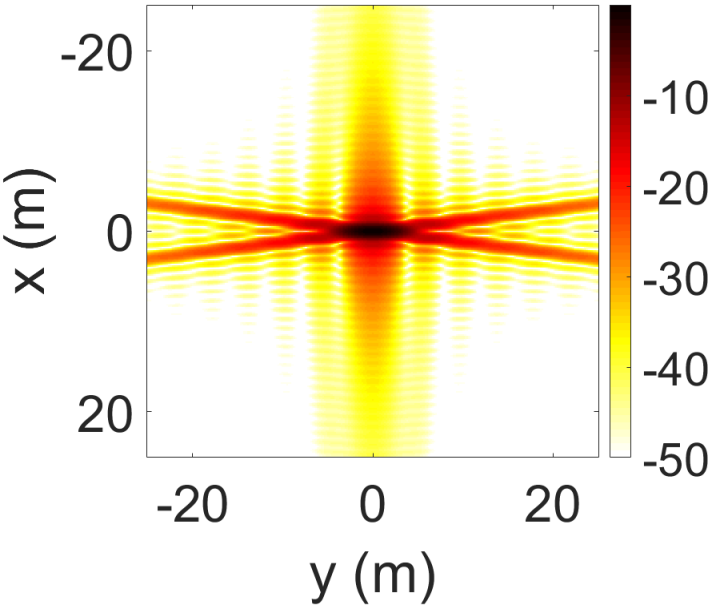

Figure 28. Single point scatter scenario SAR image of Table 5, Point 5 containing noise.

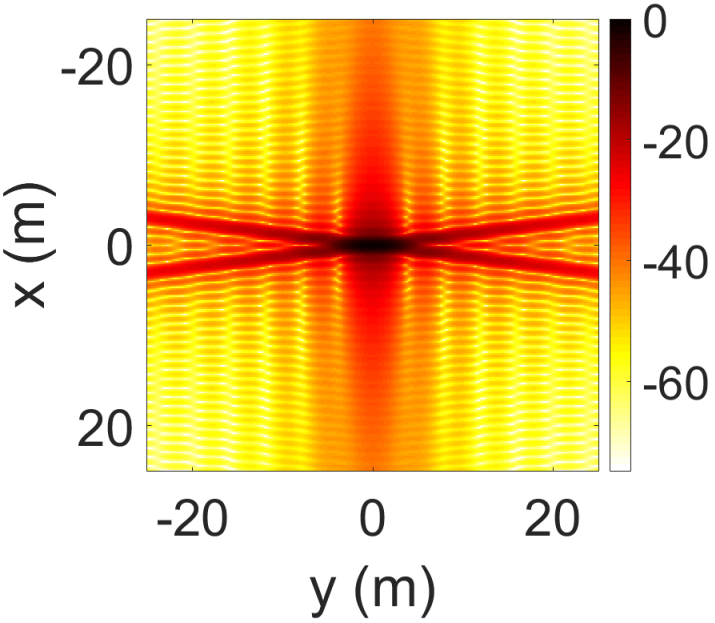

Figure 29. Single point scatter scenario SAR image of Table 5, Point 5 containing noise and increased dynamic range.

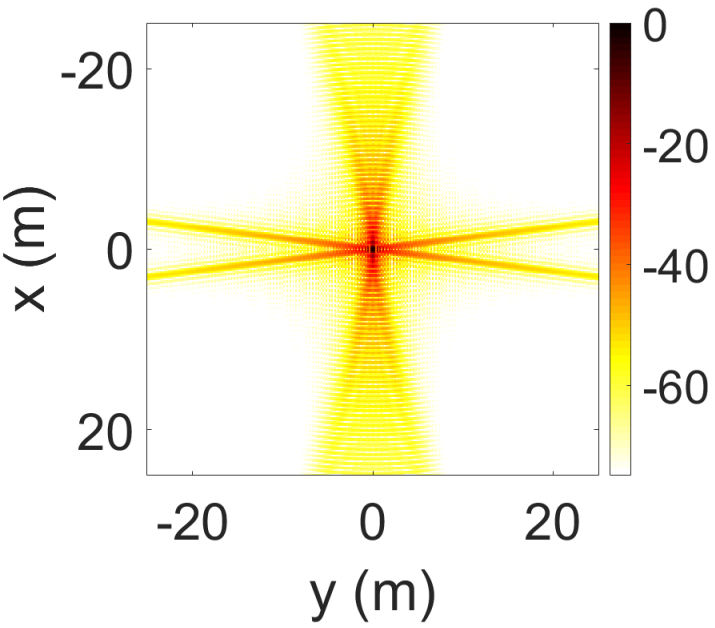

Figure 30. Single point scatter scenario SAR image of Table 5, Point 1 containing noise, increased dynamic range with decreased SNR $\approx$ 0 dB.

V. Conclusion

While there is a high interest in using communication transmitters in urban environment for passive radar, very little has been done to explore a true optimization of transmitter/receiver pairing(s) through receiver design. This research shows the feasibility of using a genetic algorithm (GA) to optimize receiver design, and the increased efficiency a GA has over previously used exhaustive search models. We have introduced a general multi-objective simulation model for bi-static multi-objective optimization across mixed variables with discontinuous, non-convex functions. Our model focuses on receiver design optimization for a constrained passive radar environment. We have shown the ability of the MOO model and related GA to operate efficiently and effectively. Because of the generality of the model and the robustness of genetic algorithms, this research is easily expanded to more complicated and convoluted optimization radar problems, specifically multi-static SAR imagery.

Future work could include the expansion of the model for multi-static SAR. Expanding the model for multi-static imagery would require objectives to be defined based on multi-static metrics that fit into the general model architecture of vectored variables. Multi-static metrics are complicated and iteratively dependent upon system geometries. If sufficient multi-static objectives can be defined, the generality of this model could easily be expanded to the analysis of all aspects in multi-static SAR imagery. The analysis could also include the impact of current assumptions widely accepted within the field namely platform location error and the variability of system parameters.

Bibliography

1. S. Sen and A. Nehorai, "Adaptive Design of OFDM Radar Signal With Improved Wideband Ambiguity Function," *IEEE Transactions on Signal Processing*, vol. 58, pp. 928–933, Feb 2010.

2. C. R. Berger, B. Demissie, J. Heckenbach, P. Willett, and S. Zhou, "Signal Processing for Passive Radar Using OFDM Waveforms," *IEEE Journal of Selected Topics in Signal Processing*, vol. 4, pp. 226–238, Feb 2010.

3. J. R. Guterrez del Arroy, J. A. Jackson, and M. A. Temple, "Receive signal processing for OFDM-based radar imaging," in *Acoustics, Speech and Signal Processing (ICASSP), 2013 IEEE International Conference on*, pp. 2775–2779, May 2013.

4. P. Krysik, L. Maslikowski, P. Samczynski, and A. Kurowska, "Bistatic ground-based passive SAR imaging using TerraSAR-X as an illuminator of opportunity," in *International Conference on Radar*, pp. 39–42, Sept 2013.

5. D. Gromek, P. Samczyski, K. Kulpa, J. Misiurewicz, and A. Gromek, "Analysis of range migration and Doppler history for an airborne passive bistatic SAR radar," in *2014 15th International Radar Symposium (IRS)*, pp. 1–6, June 2014.

6. W. Ketpan, S. Phonsri, R. Qian, and M. Sellathurai, "On the Target Detection in OFDM Passive Radar Using MUSIC and Compressive Sensing," in *Sensor Signal Processing for Defence (SSPD), 2015*, pp. 1–5, Sept 2015.

7. J. F. Gu, J. Moghaddasi, and K. Wu, "Delay and Doppler shift estimation for OFDM-based radar-radio (RadCom) system," in *Wireless Symposium (IWS), 2015 IEEE International*, pp. 1–4, March 2015.

8. M. Ummenhofer, J. Schell, J. Heckenbach, H. Kuschel, and D. W. D. Hagan, "Doppler estimation for DVB-T based Passive Radar systems on moving maritime platforms," in *Radar Conference (RadarCon), 2015 IEEE*, pp. 1687–1691, May 2015.

9. S. Stevens and J. Jackson, "Emitter selection criteria for passive multistatic synthetic aperture radar imaging," *IET Radar, Sonar Navigation*, vol. 8, no. 9, pp. 1267–1279, 2014.

10. J. P. Gauthier and A. G. Dempster, "Attitude measurement errors in bistatic SAR," in *2012 IEEE International Geoscience and Remote Sensing Symposium*, pp. 323–326, July 2012.

11. G. Lellouch and H. Nikookar, "On the capability of a radar network to support communications," in *14th IEEE Symposium on Communications and Vehicular Technology in the Benelux*, pp. 1–5, Nov 2007.

12. G. Lellouch, P. Tran, R. Pribic, and P. van Genderen, "OFDM waveforms for frequency agility and opportunities for Doppler processing in radar," in *2008 IEEE Radar Conference*, pp. 1–6, May 2008.

13. G. Lellouch, R. Pribic, and P. van Genderen, "Wideband OFDM pulse burst and its capabilities for the Doppler processing in radar," in *2008 International Conference on Radar*, pp. 531–535, Sept 2008.

14. A. Evers and J. A. Jackson, "Cross-ambiguity characterization of communication waveform features for passive radar," *IEEE Transactions on Aerospace and Electronic Systems*, vol. 51, pp. 3440–3455, Oct 2015.

15. G. E. A. Franken, H. Nikookar, and P. V. Genderen, "Doppler Tolerance of OFDM-coded Radar Signals," in *2006 European Radar Conference (EuRAD)*, pp. 108–111, Sept 2006.

16. M. Braun, M. Fuhr, and F. K. Jondral, "Spectral Estimation-Based OFDM Radar Algorithms for IEEE 802.11a Signals," in *Vehicular Technology Conference (VTC Fall), 2012 IEEE*, pp. 1–5, Sept 2012.

17. R. F. Tigrek, W. J. A. de Heij, and P. van Genderen, "Multi-carrier radar waveform schemes for range and Doppler processing," in *2009 IEEE Radar Conference*, pp. 1–5, May 2009.

18. Y. Paichard, "OFDM waveforms for multistatic radars," in *2010 IEEE Radar Conference*, pp. 1187–1190, May 2010.

19. S. Searle, J. Palmer, L. Davis, D. W. O'Hagan, and M. Ummenhofer, "Evaluation of the ambiguity function for passive radar with OFDM transmissions," in *2014 IEEE Radar Conference*, pp. 1040–1045, May 2014.

20. P. Falcone, F. Colone, P. Lombardo, and T. Bucciarelli, "Range sidelobes reduction filters for WiFi-based passive bistatic radar," in *2009 European Radar Conference (EuRAD)*, pp. 133–136, Sept 2009.

21. S. B. Weinstein, "The history of orthogonal frequency-division multiplexing [history of communications]," *IEEE Communications Magazine*, vol. 47, pp. 26–35, November 2009.

22. S. Koslowski, M. Braun, and F. K. Jondral, "Using filter bank multicarrier signals for radar imaging," in *IEEE/ION Position, Location and Navigation Symposium - PLANS 2014*, pp. 152–157, May 2014.

23. J. Brown, K. Woodbridge, A. Stove, and S. Watts, "Air target detection using airborne passive bistatic radar," *Electronics Letters*, vol. 46, pp. 1396–1397, September 2010.

24. J. R. Guterrez del Arroy, J. A. Jackson, and M. A. Temple, "WiMAX ambiguity function for PCL systems," in *Proceedings of the IEEE 2010 National Aerospace and Electronics Conference (NAECON)*, pp. 54–59, July 2010.

25. J. R. Guterrez del Arroy and J. A. Jackson, "SAR imaging using WiMAX OFDM PHY," in *2011 IEEE RadarCon (RADAR)*, pp. 129–134, May 2011.

26. J. R. Guterrez del Arroy and J. A. Jackson, "Range profiles from an experimental OFDM passive radar," in *International Waveform Diversity Design Conference (WDD)*, pp. 074–078, Jan 2012.

27. J. R. Guterrez del Arroy and J. A. Jackson, "WiMAX OFDM for passive SAR ground imaging," *IEEE Transactions on Aerospace and Electronic Systems*, vol. 49, pp. 945–959, April 2013.

28. A. Evers and J. Jackson, "Experimental passive SAR imaging exploiting LTE, DVB, and DAB signals," in *IEEE Radar Conference*, pp. 0680–0685, May 2014.

29. A. Evers and J. A. Jackson, "Analysis of an LTE waveform for radar applications," in *IEEE Radar Conference*, pp. 0200–0205, May 2014.

30. G. Lellouch, A. Mishra, and M. Inggs, "Impact of the Doppler modulation on the range and Doppler processing in OFDM radar," in *2014 IEEE Radar Conference*, pp. 0803–0808, May 2014.

31. F. Santi, D. Pastina, M. Bucciarelli, M. Antoniou, D. Tzagkas, and M. Cherniakov, "Passive multistatic SAR with GNSS transmitters: Preliminary experimental study," in *2014 European Radar Conference (EuRAD)*, pp. 129–132, Oct 2014.

32. F. Santi, M. Antoniou, and D. Pastina, "Point Spread Function Analysis for GNSS-Based Multistatic SAR," *IEEE Geoscience and Remote Sensing Letters*, vol. 12, pp. 304–308, Feb 2015.

33. F. Santi, M. Bucciarelli, D. Pastina, and M. Antoniou, "CLEAN technique for passive bistatic and multistatic SAR with GNSS transmitters," in *2015 IEEE Radar Conference (RadarCon)*, pp. 1228–1233, May 2015.

34. P. Falcone, F. Colone, C. Bongioanni, and P. Lombardo, "Experimental results for OFDM WiFi-based passive bistatic radar," in *2010 IEEE Radar Conference*, pp. 516–521, May 2010.

35. F. Colone, P. Falcone, C. Bongioanni, and P. Lombardo, "WiFi-Based Passive Bistatic Radar: Data Processing Schemes and Experimental Results," *IEEE Transactions on Aerospace and Electronic Systems*, vol. 48, pp. 1061–1079, April 2012.

36. National Telecommunications and Information Administration (NTIA), United States Department of Commerce, "Spectrum Sharing." www.ntia.doc.gov/category/spectrum-sharing, Nov 2016.

37. J. Guerci and S. Pillai, "Theory and application of optimum transmit-receive radar," in *IEEE International Radar Conference*, pp. 705–710, 2000.

38. J. Bergin, P. Techau, J. Don Carlos, and J. Guerci, "Radar waveform optimization for colored noise mitigation," in *2005 IEEE International Radar Conference*, pp. 149–154, May 2005.

39. L. Patton, D. Hack, and B. Himed, "Adaptive pulse design for space-time adaptive processing," in *2012 IEEE 7th Sensor Array and Multichannel Signal Processing Workshop (SAM)*, pp. 25–28, June 2012.

40. S. Sen, "Adaptive OFDM Radar Waveform Design for Improved Micro-Doppler Estimation," *IEEE Sensors Journal*, vol. 14, pp. 3548–3556, Oct 2014.

41. N. H. Nguyen, K. Dogancay, and L. Davis, "Joint transmitter waveform and receiver path optimization for target tracking by multistatic radar system," in *Statistical Signal Processing (SSP), 2014 IEEE Workshop on*, pp. 444–447, June 2014.

42. J. Palmer, A. Summers, M. Ummenhofer, G. Bournaka, S. Palumbo, D. Cristallini, and H. Kuschel, "Receiver platform motion estimation using terrestrial broadcast transmitters for passive radar," in *2015 IEEE Radar Conference*, pp. 151–155, Oct 2015.

43. W. C. Barott and B. Himed, "Fast wide-area P-SAR/ISAR performance prediction," in *2016 IEEE Radar Conference (RadarConf)*, pp. 1–6, May 2016.

44. R. Haupt and S. Haupt, *Practical Genetic Algorithms*. Hoboken, NJ: John Wiley and Sons, Inc, 2004.

45. K. Deb, *Multi-Objective Optimization using Evolutionary Algorithms*. Hoboken, NJ: John Wiley and Sons, Inc., 2002.

46. J. Knowles, D. Corne, and K. Deb, *Multiobjective Problem Solving from Nature*. New York, NY: Springer, 2008.

47. W. Banzhaf, P. Nordin, R. Keller, and F. Francone, *Genetic Programming, An Introduction*. San Franciso, CA: Morgan Kaufmann Publishers, Inc., 1998.

48. C. C. Coello, G. Lamont, and D. V. Veldhuizen, *Evolutionary Algorithms for Solving Multi-Objective Problems*. New York, NY: Springer, 2007.

49. K. Deb, A. Pratap, S. Agarwal, and T. Meyarivan, "A fast and elitist multiobjective genetic algorithm: NSGA-II," *IEEE Transactions on Evolutionary Computation*, vol. 6, pp. 182–197, Apr 2002.

50. N. J. Willis, *Bistatic Radar*. Silver Spring, MD: Technology Service Corporation, 1995.

51. E. Zitzler and L. Thiele, "Multiobjective evolutionary algorithms: a comparative case study and the strength Pareto approach," *IEEE Transactions on Evolutionary Computation*, vol. 3, no. 4, pp. 257–271, 1999.

52. Q. Zhang and H. Li, "MOEA/D: A Multiobjective Evolutionary Algorithm Based on Decomposition," *IEEE Transactions on Evolutionary Computation*, vol. 11, pp. 712–731, December 2007.

53. The Math Works, Inc., "Genetic Algorithm and Direct Search Toolbox 2 User's Guide." http://opencourse.ncyu.edu.tw/ncyu/file.php/30/Global_Optimization_Toolbox-User_Guide.pdf, 2009.

54. The Math Works, Inc., "Multiobjecitve Genetic Algorithm Options." www.mathworks.com/help/gads/examples/multiobjective-genetic-algorithm-options.html, September 2016.

55. C. V. Jakowatz, D. E. Wahl, P. H. Eichel, D. C. Ghiglia, and P. A. Thompson, *Spotligh-Mode Synthetic Aperture Radar: A Signal Processing Approach*. New York,NY: Springer, 1996.

56. A. V. Oppenheim and R. W. Schafer, *Discrete-Time Signal Processing*. Upper Saddle River, NJ: Pearson Higher Education, Inc., 2010.

List of Acronyms

AFIT Air Force Institute of Technology

AF-ISL ambiguity function integrated side-lobe level

ATR automatic target recognition

BSNR bi-static signal to noise ratio

DAB digital audio broadcasting

DTCR distributed target contrast ratio

DTFT discrete time Fourier transform

DVB digital video broadcasting

EMRA effective multi-static resolution area

FCC Federal Communications Commission

GAMOO genetic algorithm multi-objective optimization

GIQE general image quality equation

GA genetic algorithm

GP genetic programming

IEEE Institute of Electrical and Electronics Engineers

I-SAR inverse synthetic aperture radar

ITU International Telecommunication Union

LTE long term evolution

MME motion measurement error

MOEA multi-objective evolutionary algorithms

MOO multi-objective optimization

MSAR multi-static synthetic aperture radar

MSNR multi-static signal to noise ratio

NCGA neighborhood cultivation genetic algorithm

NCM neighborhood constraint method

NPGA niched Pareto genetic algorithm

NPGA2 niched Pareto genetic algorithm 2

NSDE non-dominated sorting differential evolution

NSGA non-dominated sorting genetic algorithm

NSGA-II non-dominated sorting genetic algorithm II

NSMA non-dominated sorting memetic algorithm

NSTEA non-inferior surface tracing evolutionary algorithm

NTIA National Telecommunications and Information Administration

OFDM orthogonal frequency multiplex division

OMOEA orthogonal multi-objective evolutionary algorithm

OMOEA-II orthogonal multi-objective evolutionary algorithm II

PBR passive bi-static radar

PBSAR passive bi-static synthetic aperture radar

PCGA Pareto converging genetic algorithm

PMOGA parallel multi-objective algorithm

PMOHYPEA parallel evolutionary multi-objective optimization using hypergraphs evolutionary algorithm

PMSAR passive multi-static synthetic aperture radar

PSAR passive synthetic aperture radar

PSF point spread function

PTCR point target contrast ratio

RCS radar cross section

SAR synthetic aperture radar

SNR signal to noise ratio

UHF ultra high frequency

VHF very high frequency

WGN white Gaussian noise

WiMAX world wide interoperability for microwave access

REPORT DOCUMENTATION PAGE

Form Approved
OMB No. 0704–0188

1. REPORT DATE *(DD–MM–YYYY)*	2. REPORT TYPE	3. DATES COVERED *(From — To)*
14–09–2017	Master's Thesis	Jan 2016 — Sept 2017

4. TITLE AND SUBTITLE

Genetic Algorithm Receiver Optimization For Passive, Bi-static Synthetic Aperture Radar

5a. CONTRACT NUMBER

5b. GRANT NUMBER

5c. PROGRAM ELEMENT NUMBER

6. AUTHOR(S)

Chamberlain, Chad Nile, Major, USAF

5d. PROJECT NUMBER

5e. TASK NUMBER

5f. WORK UNIT NUMBER

7. PERFORMING ORGANIZATION NAME(S) AND ADDRESS(ES)

Air Force Institute of Technology
Graduate School of Engineering and Management (AFIT/EN)
2950 Hobson Way
WPAFB OH 45433-7765

8. PERFORMING ORGANIZATION REPORT NUMBER

AFIT-ENG-MS-17-S-007

9. SPONSORING / MONITORING AGENCY NAME(S) AND ADDRESS(ES)

Undisclosed

10. SPONSOR/MONITOR'S ACRONYM(S)

11. SPONSOR/MONITOR'S REPORT NUMBER(S)

12. DISTRIBUTION / AVAILABILITY STATEMENT

DISTRIBUTION STATEMENT A:
APPROVED FOR PUBLIC RELEASE; DISTRIBUTION UNLIMITED.

13. SUPPLEMENTARY NOTES

14. ABSTRACT

Utilizing communication transmissions within an urban environment for passive radar has seen a huge surge in interest over the past decade. While the feasibility of using signals of opportunity for passive radar has been shown, very little research has been done for the optimization of passive transmitter/receiver pairings within urban environments. This research provides a receiver design based optimization of passive transmitter/receiver pairing using non-dominated sorting genetic algorithm II (NSGA-II) to solve a constrained multi-objective model. Comparing the results of an exhaustive search and the genetic algorithm (GA), the efficiency and effectiveness of using a GA for mixed variables over non-continuous, non-convex objectives associated with bi-static synthetic aperture radar (SAR) is demonstrated.

15. SUBJECT TERMS

Passive, Bi-static, SAR, Genetic Algorithm, Receiver, Optimization

16. SECURITY CLASSIFICATION OF:			17. LIMITATION OF ABSTRACT	18. NUMBER OF PAGES	19a. NAME OF RESPONSIBLE PERSON
a. REPORT	b. ABSTRACT	c. THIS PAGE			Dr. Julie A. Jackson, AFIT/ENG
U	U	U	U	81	19b. TELEPHONE NUMBER *(include area code)* (937) 255-3636, x4678; julie.jackson@afit.edu